POLITECNICO DI TORINO

Department of Mechanical and Aerospace Engineering

Master's degree course in Aerospace Engineering

Master's Degree Thesis

Simplified structural fragmentation analysis of space debris subjected to destructive re-entry in the atmosphere

Supervisor
Prof. Paolo Maggiore
Prof. Salvatore Brischetto

Candidate
Pasquale Megliola

Company supervisor
Dott. Roberto Destefanis
Dott. Simone Bianchi

July 2019

To
my grandparents, my
family and F. Russo

Abstract

Thales Alenia Space in Italy (TASinI) in Turin had been developed a software for destructive reentry in the atmosphere named TADAP (Trajectory and Aerothermodynamic Debris Analysis Program) to the evaluation of the likelihood of a satellite's ground impact. A relevant development of this software would be inclusion of a structural model that require reliable results on the structural analysis of the satellite but with small calculation times.

Therefore, the aim of this project was to find a possible simplification of the current FEM structural analysis, which requires high calculation times for the analysis of the entire satellite if it is performed at any moment of re-entry in the atmosphere.

In order to have the stress values for comparison and to understand the structural behaviour of some components of the satellite, since there is no data concerning the loads or the stress on a satellite during re-entry, three components were analyzed:

- A ceramic bench, inside the satellite and difficult to thermally demise during re-entry also because made of ceramic material;
- A special washer made of a zinc-based alloy (EZAC^{TM}), part of the Demisable Joint (TASinI patent);
- The Demisable Joint, a solution to improve the demisability of the satellite, by facilitating the detachment of the external panels, improving the exposure of inner components to heat flux and thus increasing their demisability;

From the results of FEM analysis on the study cases it’s clear that each component withstands at operative loads without breaking-up but they have a different behaviour at the atmospheric re-entry. The bench breaks between 80 and 90 km with peak of stress where there is the maximum temperature gradient and near the hole. The washer has peak of stress near the slot of the cleat and in the upper part in contact with the head of the screw, where is the preload, but it doesn’t entry in plastic field during his operative orbit lifetime at 100 km.

The FEM analysis on the study cases show the structural behaviour of some components during atmospheric re-entry and give a reference to simplify the existing structural models.

Contents

1. Introduction

This chapter analyzes the problem of atmospheric re-entry from historical background and the problem represented by space debris and their influence on safety in term of on-ground risk.

Significant importance is given to analytic studies on that problem and how they are faced, considering some specific tools.

1.1. Space debris and re-entry predictions

Satellites in orbit around Earth are used in many areas and disciplines, from remote sensing to communications and other purposes. In the last decades, due to increasing of space activities, the number of objects no longer in use has risen, creating a huge number of debris that can be dangerous for other space missions.

In almost 50 years of activities, more than 4900 launches have placed 6600 satellites into orbit of which about 3600 remain in space; only a small fraction of them, about 1000, are still operational. Just 6% of the catalogued orbital populations are operational spacecraft, while 38% can be attributed to decommissioned satellites, upper stages and mission-related objects (launch adaptors, lens covers, etc.).

Not all of these objects are still intact; in fact, a lot of collisions, explosions and fragmentations have been recorded from the beginning of the Space Era, generating a large population of objects larger than 1 cm. Orbits are further changed by perturbations (which in LEO include unevenness of the Earth's gravitational field), collisions can occur from any direction. For these satellites, it may take many years for these pieces to return to Earth while higher-altitude satellites are of less concern because they can stay in orbit much longer. The majority of debris can be located at altitudes from 800 to 1000 km, i.e. included in LEO orbits range.

This space debris pollution has a huge impact on the operation of active spacecraft (for example, the ISS had to perform 7 evasive maneuvers up to 2003 and 9 more in August

2008). Based on the prediction of future world launch activity, on-orbit explosions and collisions, future solar cycle activity, effect of mitigation strategies and the effect of protection methods, the future of the LEO space debris environment can be predicted, even if the impact of mega-constellations hasn't deeply identified. The long-term simulations seem to show that, even with no new launches from now on, debris in LEO will continue to increase due to collisions. The active removal of several large objects could be helpful, but the effectiveness and feasibility of this measure is nowadays under investigation. Hence, the only feasible option currently available is to adopt mitigation measures (as, for example, passivation of satellites at the end of their operational life, and End of Life de/re-orbiting) to avoid the increasing of the debris population.

Figure 1- Satellite distribution in 2015

It is very difficult to predict where debris, from a randomly re-entering satellite, will hit because drag is directly proportional to atmospheric density that changes greatly at different altitudes. Reportedly, only one person has ever been hit by debris from a re-

entering satellite and, fortunately, she was not injured because the fragment was too small. In 1997, Lottie Williams was walking in a park in Tulsa, Oklahoma, when she was hit on the shoulder by a piece of metal. The metal was later confirmed to be a piece of a Delta II rocket.

Even if predictions, performed with dedicate tools and software are affected by a natural uncertainty, the risk posed by re-entering artificial objects is lower than other hazards, however the great space activity in LEO orbits and the importance the space industries reserve to safety imposes an increasing attention on this phenomenon.

The growing concern for the debris pollution of the Earth's orbital environment is reflected by the number of relevant guidelines and regulations set forward by national or international organizations.

In 1993, the Inter-Agency Debris Coordination Committee (IADC) was formed as a forum for technical exchange and coordination on space debris matters and is now composed of 13 national Space Agencies. In 2002, IADC published the "Space Debris Mitigation Guidelines" which were presented to the Scientific and Technical Subcommittee of the United Nations' Committee on the Peaceful Uses of Outer Space (UNCOPUOS) and served as baseline for the "UN Space Debris Mitigation Guidelines", published in 2007 and approved by 63-member nations as voluntary high-level space debris mitigation measures. The IADC guidelines were updated in 2007 (IADC-02-01, Revision 1, September 2007) and in 2019 (under publication).

Several nations and organizations have developed mandatory Space Debris mitigation requirements. For instance, in 2008, ESA published the "Space Debris Mitigation for Agency Projects". The requirements were made applicable to all space vehicles, including launchers, satellites and inhabited objects. The document was updated in 2014 (ESA/ADMIN/IPOL (2014) 2) and its validity extended in 2018 until March 2022.

In June 2008, Space Debris Mitigation requirements were made applicable as part of the "French Loi relative aux Opérations Spatiales" (LOS, N°2008-518). The French LOS has been updated on July 11th, 2017.

ISO International debris standards were developed since 2003 by the ISO TC20/SC14 committee "Space systems and operations", composed by members representing 13 countries. The ISO key document is the "ISO 24113 - Space Debris Mitigation". This standard (published in July 2010, 1st edition; May 2011, 2nd edition) is based on the IADC and UN guidelines, and aims at translating the existing recommendations into quantitative implementation requirements. An updated version of the ISO 24113 is under publication.

The European Cooperation for Space Standardization (ECSS) supports the development of standards within ISO TC20/SC14 development and published the ECSS-U-AS-10C Adoption Notice of ISO 24113: Space systems - Space debris mitigation requirements in 2012. The European Committee for Standardization (CEN) published the ECSS-U-AS-10C Adoption Notice of ISO 24113 as EN 16604-10 in 2014. Also the ESA document "Space Debris Mitigation Policy for Agency Projects" is based on the ECSS-U-AS-10C and therefore on the ISO 24133.

Regarding the re-entry risk, the ESA policy document 2 states that, for ESA Space Systems, the casualty risk shall not exceed 1 in 10,000 for any re-entry event (controlled or uncontrolled). If the predicted casualty risk for an uncontrolled re-entry exceeds this value, an uncontrolled re-entry is not allowed, and a targeted controlled re-entry shall be performed.

1.2. Atmospheric re-entry description and history

Atmospheric re-entry, for definition, is a process by which vehicles from outside the atmosphere of a planet enter in the atmosphere itself and potentially hit planetary surface. Re-entry occurs in 3 ways:

- **Uncontrolled:** the spacecraft re-enters after a natural decay, from 120 km altitude the re-entry usually takes more than one orbit;
- **Semi controlled:** the spacecraft re-enters after a partially-guided de-orbit, from 120 km altitude, the re-entry usually takes less than one orbit;

- **Controlled entry:** the spacecraft re-enters after a totally-guided de-orbit, from 120 km altitude the re-entry usually takes less than one orbit, eventually targeting a specific area (e.g. unpopulated oceanic area);

As said, 120 km is the usually-assumed altitude as starting point of simulation, below this value the re-entry is supposed to take place in few orbits or less.

During the aero-breaking process in the atmosphere, the initial potential and kinetic energy of the spacecraft is converted into thermal energy that is consumed by the ambient atmosphere and by the spacecraft itself. The resulting thermal and mechanical loads will destroy (fragment and/or demise) the spacecraft completely or partially.

Figure 2- Artist's impression of ATV-5 breakup and re-entry (ESA-D. Durcos)

In the first case, destruction may occur by:

- Fragmentation, generating two or more children objects from a parent body.
- Deformation, caused by torque, bending, buckling or by thermal stress.
- Bursting, for example by internal pressure increase during re-entry.
- Complete destruction, by phase change or chemical reaction like melting and evaporation.

The technology of atmospheric re-entry was a consequence of the World War II and Cold War. Researches on ballistic missiles and nuclear weapons have been led by the Soviet Union and the United States to further the military capability of those technologies. Actually, in order to use a nuclear missile, it was necessary to develop the technology for atmospheric re-entry because calculations showed the kinetic energy of a nuclear warhead returning from orbit was sufficient to completely vaporize the warhead.

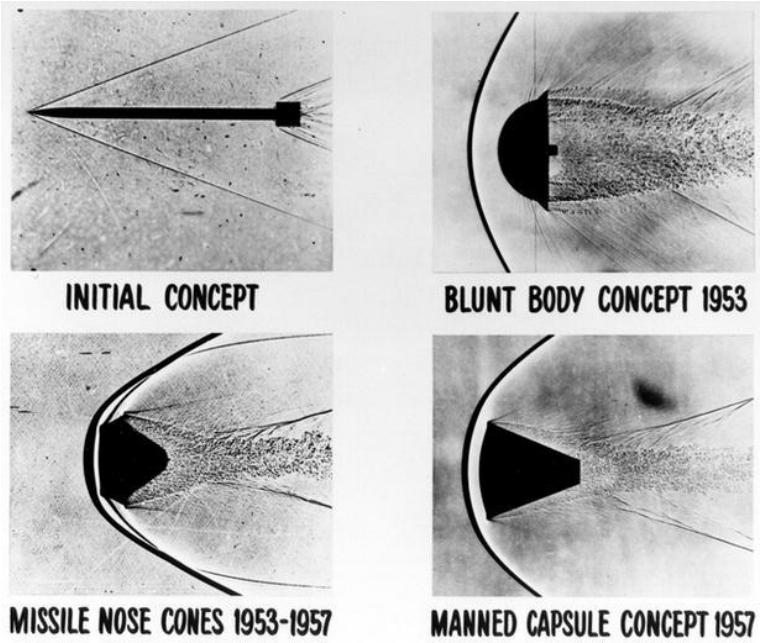

Figure 3- Blunt body concepts

In 1952, H. Julian Allen and Alfred J. Eggers of the National Advisory Committee for Aeronautics (NACA) discovered that a squat body was the most efficient shape for a heat shield and showed that the heat generated was inversely proportional to the coefficient of resistance, namely higher is this coefficient, lower is the heat. Through this shape, the shock wave and the shock layer are pushed away from the wall of the vehicle. Since most of the hot gasses do not come into direct contact, the heat energy remains enclosed in the gas and moves around the vehicle to dissipate later in the atmosphere. This discovery, which initially was treated as a military secret, was published in 1958.

The theory of the blunt body made possible the design of heat shields used for the capsules in programs Mercury, Gemini and Apollo to ensure the survival of the astronauts during atmospheric reentry to the Earth.

The technology was further pushed also for propaganda and military advantage in pursuing space exploration by the Soviet Union. The achievement of Jury Gagarin successfully returning safely to Earth was reached indeed through atmospheric re-entry technology. The United States saw the Soviet Union's progresses as a challenge to its national pride as well as a threat to national security, causing the increasing of Space Program and the beginning of the Space Race.

After the Shuttle era, during which many problems related to atmospheric re-entry were dealt with, a strong attention is currently focused on destructive re-entry, typically of unmanned S/Cs.

1.2.1. Debris analysis tools

During the last decades re-entry analyses and ground risk assessment have become an important topic that space agencies and research institutes have developed tools to evaluate this process.

This analysis requires the geometric and physical models of the object and of its elements. To describe the destruction during re-entry some aspects have to be considered such as flight dynamics of the vehicle, aerodynamic and aerothermal loads, dynamic spacecraft behavior, local heating and the melting process, mechanical loads and the relevant fragmentation and deformation processes and fragment tracking until impact, but regard to mechanical loads actually there aren’t any studies. The development of analysis tools for spacecraft destruction started about 10 years ago with the activities for space debris mitigation. There are a few number of codes and analysis methods, they can be divided into two categories: object-oriented codes and spacecraft-oriented codes.

Figure 4- Destructive re-entry of TRMM Spacecraft

1.2.1.1. Object-oriented codes

Object-oriented codes analyze only single parts of the spacecraft. These methods assume that at a certain altitude, usually in the range between 75 and 85 km, the spacecraft breakups into its individual critical elements and for each of them a destructive re-entry analysis is then performed. This concept allows determining a ground impact footprint for the surviving debris objects that depends on breakup conditions (position, altitude, velocity vector) and on the ballistic coefficients of the debris objects. Due to this simplification, only the critical parts of the spacecraft must be modeled, reducing strongly the geometry. In all those methods, the component's unique information available is basic geometry, size, mass and material. Therefore, object-oriented codes are not able to analyze a complete spacecraft with full dynamics, heating of external parts and the internal protection.

The main object-oriented simulation software are the following:

- **DEBRISK:** Developed by CNES ("Centre National d' Etudes Spatiales") [7], this tool is a software that outputs trajectories of the various re-entering components, the surface heat load and the debris demise altitude. The tool is efficient and fast

because it models simple shapes (spheres, boxes, flat plates and cylinders) and common materials. During the descent, the wall heat loads are integrated to obtain the surface temperature. In case of melting, layers are peeled off, adjusting the shape until demise occurs. The core of the software is the simple temporal integration of the equation of motion for complete satellite from the entry point until break-up and the fragments, from break-up altitude to the demise altitude or ground impact. Each independent object is simulated using an aerodynamic model to obtain drag coefficient, a thermal model to estimate heat transfer to the surface of the object, an ablation model to determinate the amount of material ablated and the propagation of the re-entry path.

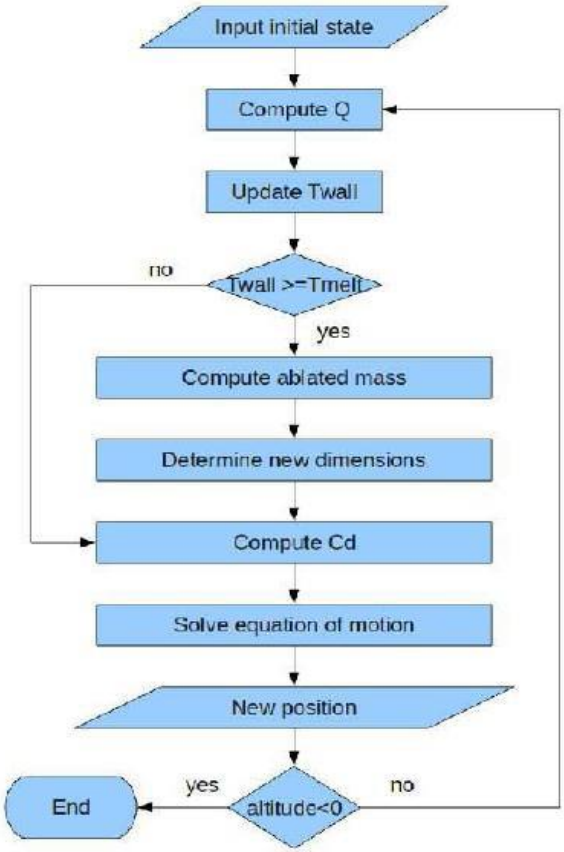

Figure 5- DEBRISK flow chart

- **DRAMA:** Developed by ESA ("European Space Agency") [13], it is the acronym of "Debris Risk Assessment and Mitigation Analysis". This supporting tool will

assist ESA futures space programs in performing orbital debris assessments in compliance with the requirements on Space Debris Mitigation for ESA projects. It is capable to predict the debris and meteoroid flux on a sphere, or on an oriented plate, for a given target object. It also determinates the probabilities of shielding for different designs and impact level, to predict the number of avoidance maneuvers of an operational spacecraft for given collision object sizes and corresponding orbit uncertainties, to realize the implementation of the de-orbiting procedures at the end-of-life. It gives prediction of orbital lifetimes and analyze atmospheric re-entry of an object.

- **TADAP:** Developed by TASinI ("Thales Alenia Space in Italy"), it is the acronym of "Trajectory and Aerothermodynamic Debris Analysis Program". The following software is useful to analyze the destructive reentry of satellites and to trace the various debris mitigation, considering their trajectory and modelling them with simple shapes such as: spheres, cylinders, flat panels or boxes. This software is very versatile and can simulate whole complex satellites, taking in input its geometry, material, trajectory and external conditions and giving in output its defragmentation and an approximate area of impact with the earth's soil. This software is written in MATLAB code and implements both aerodynamic and aerothermodynamic models by iteratively analyzing an object during its reentry into the atmosphere.

1.2.1.2. Spacecraft-oriented codes

Spacecraft-oriented codes model the complete spacecraft as close as possible to the real design of one consistent object. Due to spacecraft complexity, there is only two codes available and this are SCARAB ("Spacecraft Atmospheric Re-Entry and Aerothermal Breakup"), developed by Hyperschall Technologie Göttingen (HTG) and PAMPERO developed by CNES ("Centre National d'Etudes Spatiales").

The SCARAB software [4] has a graphical modeling system with distinct hierarchy levels, which allow to create complex. The modeler provides for each construction element the mass, the center of mass location and the moment of inertia matrix, giving as output a complete panelized and consistent geometric model of the spacecraft.

The material database of SCARAB contains about 20 physical properties that are temperature independent like density, melting temperature, and heat of melting. Temperature-dependent properties are ultimate tensile strength, elasticity module, specific heat capacity, thermal conductivity, and emission coefficient. The re-entry trajectories and the attitude motion of the spacecraft and the later-on generated fragments are calculated by numerical integration of the full 6 degrees-of-freedom equations of motion.

Hypersonic approximations are used for the aerodynamic model, distinguishing between the three flow regimes, with an aerodynamic model. Each of these models are applied locally to the panels of the geometric element to determinate aerodynamic coefficients and to predict with the aerothermal model the convective heat transfer to the outer surface of the spacecraft. The heat transfer is computed as a combination of the free molecular and continuum values. Destruction by melting is analyzed panel by panel, if parts of the spacecraft lost connection a fragment is generated, and it is analyzed until it demises completely, fragmentizes again, or reaches the ground.

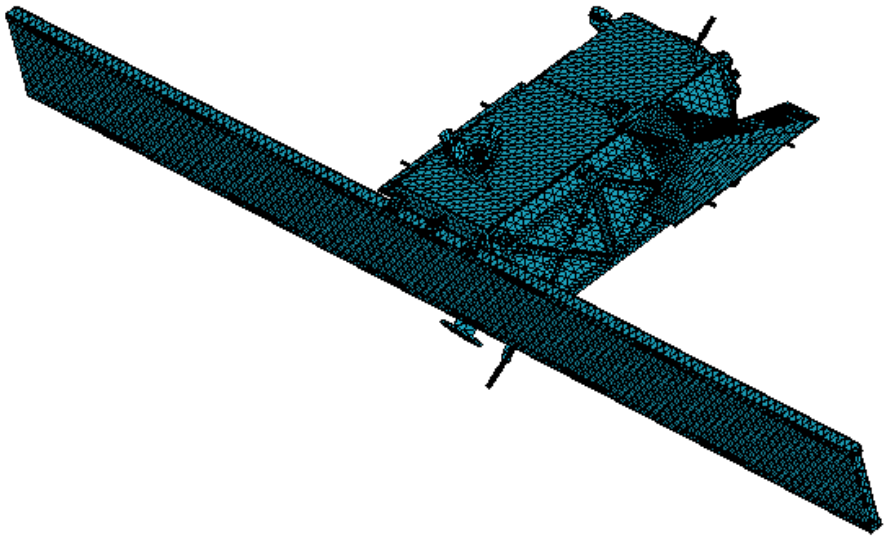

Figure 6- Sentinel 1-A model generated with SCARAB

The PAMPERO software [2] has been developed by CNES to calculate the entire trajectory of an object by 6 DOF ("Degree Of Freedom") simulations, coupled with a 3D thermal module and ablation in continuum or rarefied regime.

The trajectory and altitude of the object are integrated with Runge-Kutta method, while aerodynamic forces are due to pressure effects and inertia moments are assumed constant.

The pressure coefficient can also be calculated for 3 regimes and convective flux is estimated by empirical laws or correlations with CFD.

This tool uses a tetrahedral mesh, considering connection between surfaces or volumes for each time steps, to describe the entire reentry of the object since it is ablated.

A preliminary ablation module has been implemented in PAMPERO considering a cell removed when its melting temperature is reached.

This software simulates as real as possible an entire spacecraft model understanding various physical phenomena during the reentry.

2. Project Purpose

The aim of this work is the identifications of the main aspects needed for the implementation of structural evaluations in the current destructive re-entry tools. In particularly the activity considers the main approaches to structural analysis, the potential solutions for the re-entry, identified with specific study case via detailed FEM analyses and dedicated test activity.

The difficulty of this study is that all the structural analysis on the satellites were carried out at the launch where the loads (notably in terms of direction) are known, easier to consider and therefore to be applied to the CAD model of the satellite, while during the re-entry the loads and the structural response of the spacecraft are basically unknown (e.g. due to the difficult-to predict tumbling rate, etc.).

To implement a structural model in TADAP it is important to have the distribution of loads on different objects, therefore in this project some study cases were analyzed and later discussed, to get data of the behavior of interesting components during re-entry:

- An optical bench, difficult to burn in the atmosphere because it is inside the satellite and it is made of Silicon Nitride (a ceramic material) with high point of melting;
- A demisable joint and a washer which must be easy destruction to allow the joint to detach itself and open the external panels to disintegrate the satellite at high altitude, 90/95 km, and not subsequently as not falling down on the soil; however the washer must resists to the operational loads in orbit and therefore not give in during the satellite's operational life to complete the mission for which it was carried out.

For this structural analysis, FEM method analysis, have implemented different resistance criteria to be compared to define the behaviour of the various study cases.

It is the first time that this kind of project is carried out. The reason is given principally by the difficulty to find information about the satellites, particularly about internal

schemes, that are often very old and in certain cases covered by industrial secret. The existing simulation tools have also a limited reliability that is object of discussion.

Figure 7- Pressure tank recovered in South Africa

As said, the principle aim of this project is to analyze the atmospheric reentry of a satellite focusing on structural behavior when is subjected to load as: aerodynamic forces, pressure or others that can depend on temperature and how material properties change with temperature. In fact, there are few structural analyses on a satellite during its reentry in the earth's atmosphere, so it's important to study a component internal to a satellite how break-up if subjected to thermal, pressure, inertial loads over or also under its melting temperature.

The most real structural analysis that can be done on a satellite are with a FEM (Finite Element Method) or also known as FEA (Finite Element Analysis) using tools like Patran/Nastran and comparing the results with properties of materials, as equivalent maximum stress of breakup selected with different criteria that are listed below.

3. Structural analysis points

In this chapter are considered every step to run a structural analysis applied to destructive re-entry study cases.

3.1. Input FEM analysis

The first input in a FEM analysis is the material of the component to describe its behavior as function of its property.
Materials used in space must have high strength to weight ratio to be as efficient as possible with low weight, have good resistance at high temperatures to withstand heat streams generated by friction with various layers of the atmosphere, low sensitivity to stress corrosion and high fatigue and shock resistance with low speed of deflect growth.
There are a wide variety of materials used that respect the characteristics up listed, but satellites are usually made to be extremely light weight, using materials as titanium and aluminum, additionally they use composites and alloys such as nickel-cadmium or aluminum-beryllium. Rockets also use a base of aluminum or titanium to have light weight and may also be coated in a thermal protection system to reduce friction and heat during reentry, like a satellite.

The principle ones can be divided in:

- Extra-light alloys (like magnesium alloys);
- Light-alloys (such as aluminum and titanium);

The first type of materials can be used as plates to support internal components, while the other one, light-alloys, are generally used for more stressed structural components.

3.1.1. Magnesium alloys

Pure magnesium is not a sufficiently resistant material therefore for an industrial use, it is bonded with other elements, in order to achieve certain characteristics and a high strength-weight ratio. Magnesium alloys are the lightest materials existing nowadays, so

fall into the extra-light kind of alloy with an excellent coilability and machinability to machine tools. Due to these characteristics and the good resistance in different environments and temperatures it has collect the interest of sectors like aerospace because it is able to guarantee a lowering of consumption thanks to the considerable decrease in weight. Magnesium also has good vibration damping capabilities contributing to the increase in the life of components.
To form the magnesium alloys, there is about 80% of magnesium with 10% of aluminum and 2/5% of zinc to have the following properties:

- Specific weight γ = 1.8 Kg/dm^3
- Breakup stress σ = 58Kg/mm^2
- Percentage elongation at breakage A_P=10/15%

Unfortunately, magnesium is difficult to form/work and easily inflammable, so it must be worked in an inert atmosphere to be tied to the various elements and create the alloys. Usually they can be used for squat and little stressed elements, such as support arms or not much stressed plate.

3.1.2. Aluminum alloys

Pure aluminum has scarce mechanical properties and to be used in the structures it is necessary to alloy elements with it. The aluminum alloys are part of light-alloys and the most used in space industries are:

- DURAL-2024 (Al+Cu)
- ERGAL-7075 (Al+Zn)

The differences between the two alternatives are that the aluminum alloys 2000 are more fatigue resistant and used for external panels, the series 7000 instead are more resistant to concentrated loads and therefore used for internal reinforced structure of the satellite.

3.1.2.1. DURAL 2024

DURAL is an aluminum alloy of the 2000 series, composed of aluminum for the most part, with about 90%, and copper at 4/5% plus other alloy elements as 1,5% of magnesium and 0.6% of manganese, with the following characteristics:

- Specific weight $\gamma = 2.8$ Kg/dm^3
- Breakup stress $\sigma_R = 40/45$ Kg/mm^2
- Yield stress $\sigma_S = 30$ Kg/mm^2
- Elastic modulus E=7000/7300 Kg/mm^2
- Percentage elongation at breakage A_P =12/18%

The presence of copper increases the mechanical resistance, but it causes the corrosion of the material and this problem is could be avoid thanks to the use of aluminum with high degree of purity on surface of the body. The DURAL is generally used in the aerospace sector for the realization of the exterior cladding panels of satellite.

3.1.2.2. ERGAL 7075

ERGAL is an aluminum alloy of the 7000 series, composed of aluminum for about of 90% and zinc at 3,5/4%, also it is alloys to other elements like 1,2/2 of magnesium and 0,3 of manganese, with the following characteristics:

- Specific weight $\gamma = 2.8$ Kg/dm^3
- Breakup stress $\sigma_R = 55/65$ Kg/mm^2
- Yield stress $\sigma_S = 40/45$ Kg/mm^2
- Elastic modulus E=7000/7300 Kg/mm^2
- Percentage elongation at breakage A_P = 7/11%

ERGAL unlike the DURAL turn out to be more resistant, but for the presence of zinc has however problems of corrosion that can be solved by adding of allegiants as silver. The ERGAL for its high mechanical strength and low density is used for a lot of stressed components like the reinforcement structure of the satellite.

The aluminum alloys are difficult to weld and the mechanical characteristics are degraded around 100/200 °C, they are also easily oxidized with consequent formation of rust that subjected to tension leads to cracks.

3.1.3. Titanium alloys

The titanium alloys are very light so reentry in the category of light alloys and they are composed mostly of 90% titanium with 6% of aluminum to increase mechanical strength and vanadium or chromium at 4% to stabilize the beta phase that resists better to low temperature stresses, which corresponds to the most commonly used alloy Ti-6Al-4V, with the following mechanical characteristics:

- Specific weight $\gamma = 4{,}5$ Kg/dm^3
- Breakup stress $\sigma_R = 100/200$ Kg/mm^2
- Elastic modulus E=10500 Kg/mm^2
- Percentage elongation at breakage $A_P = 10/15\%$

They are very durable but expensive, easily oxidized on the surface and they have many porosities inside the material itself. Usually, these alloys are used in the aerospace sector for thermally and mechanically stressed components as in the realization of thermal protections or propellant tanks.

3.2. Structural models

The structural models are used for the structural analysis of a component to approximate its shape and therefore to evaluate exact stresses and so displacements of the whole structure considering two-dimensional models like the beam or the rod or two-dimensional models such as the membrane or the semi-shell, for three-dimensional components, the overlap of 1D and 2D models is considered. Depending on the shape and behavior of the element to be analyzed, it is selected the most suitable structural model to perform a correct structural analysis.

3.2.1. 1D Models

The models 1D and therefore one-dimensional, generally consider the size on which the body develops which is usually along the z axis, with the other two dimensions negligible compared to the same, for example for the structural models beam or rod depending of the load condition used there are two different conditions of stress and consequently of internal tensions, which lead to different characteristics in the deformation and so displacements.

3.2.1.1. Beam

In the beam model is considered an elongated solid that as previously exposed has a preponderant dimension compared to the other two that are neglected. The beam model is characterized by a precise condition of applied external loads that affect the internal stresses expressed in terms of bending moment, shear and normal strain.

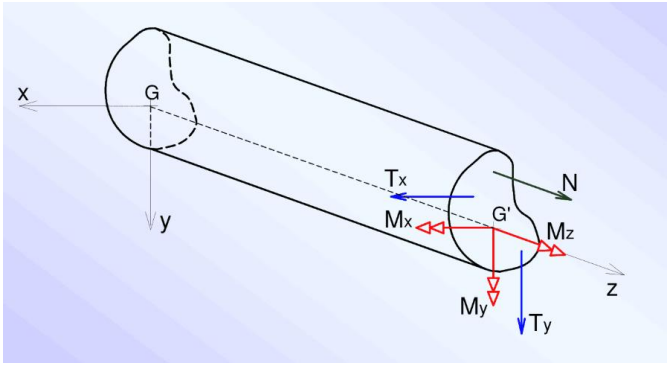

Figure 8– Beam representation with axis convection

The representation of a generic beam section is shown in Figure 8 with the resulting loads expressed as:

- Normal stress along z:

$$N_z = \int_A \sigma_{zz} \cdot dA$$

In which σ_{zz} is the normal stress acting perpendicularly to the cross section of the beam area A.

- Shear stress along y:

$$T_y = \int_A \tau_{zy} \cdot dA$$

Where, τ_{zy} indicates the shear stress agent on the cross-section of the beam that has a normal vector z-axis and in the direction of the y-axis.

- Shear stress along x:

$$T_x = \int_A \tau_{zx} \cdot dA$$

Where τ_{zx} represents the shear stress agent on the cross-section of the beam that has a normal vector z axis and in the direction of the x-axis

About the moments, they are defined positive by rotating counterclockwise by placing in the positive direction of the axis around which they are considered and are defined as:

- Bending momentum around x:

$$\mathrm{M}_x = \int_A \sigma_{zz} \cdot y \cdot dA$$

- Bending momentum around y:

$$\mathrm{M}_y = \int_A \sigma_{zz} \cdot x \cdot dA$$

- Twisting momentum around z:

$$\mathrm{M}_z = \int_A \left(\tau_{zy} \cdot x - \tau_{zx} \cdot y\right) dA$$

Considering the condition of a beam with loads distributed along beam axis, the loads are function of the Section considered and therefore of the position relative to the z-axis. By focusing on an infinitesimal element of the beam section you have the following reports:

- Distributed load in z direction:

$$p_z = -\frac{dN_z}{dz}$$

- Distributed load in y direction:

$$q_y = -\frac{dT_y}{dz}$$

- Distributed load in x direction:

$$q_x = -\frac{dT_x}{dz}$$

Only for the condition of distributed loads are valid the following assumptions:

$$\frac{dM_y}{dz} = T_x$$

$$\frac{dM_x}{dz} = T_y$$

$$\frac{dM_z}{dz} = 0$$

In the beam model with distributed loads it is assumed that the torque momentum is constant along the axis of the beam and that the bending moment around y is caused by the presence of the shear load in the x direction, while the bending moment around x is due to the shear load in the direction y.

3.2.1.2. Rod

The model of the rod assumes that it is subject only to axial loads, in particular compression ones, and is used to form generally reticular structures, considering the level of load for which the system becomes unstable, sagging.
From the analysis of an element of the rod we can get the linearized bending moment tied to the flexural stiffness of the curvature as:

$$M = E \cdot J \cdot K$$

In which E is the elastic modulus of the material, J the moment of inertia and $K = -w_{,xx}$ bending flexural stiffness.

From the equilibrium of the forces in the elementary dressed stone results:

- $\frac{dH}{dx} = 0 \rightarrow H = costante$
- $\frac{dV}{dx} = 0 \rightarrow V = costante$

Therefore, they are the normal and constant cutting efforts along x for each section. From the equilibrium of the moments, the equation of equilibrium is the following:

$$\frac{d^2M}{dx^2} + H\frac{d^2w}{dx^2} = 0$$

Where w is the vertical displacement of the average line relative to the starting position. Considering the boundary conditions, with the extremes hinged to the extremes for x = 0, L:

$$w = M = 0$$

$$H = -P = -\lambda P_0$$

From the consideration of the previously illustrated equations the critical load gets for which an auction goes in buckling given by:

$$P_{cr} = \lambda P_0 = EJ\frac{\pi^2}{L^2}$$

From which:

$$\sigma_{cr} = \frac{P_{cr}}{S} = EJ\frac{\pi^2}{L^2 S}$$

Where:

$$\begin{cases} J = \rho^2 S \;\; Inertia\ momentum \\ A = \dfrac{L}{\rho}\ Rod's\ slenderness \end{cases}$$

With ρ the minimum radius of inertia, S the area in section and L the length of the rod. Substituting the relationships of the moment of inertia and the slenderness in the σ_{cr}, the dependence of the critical stress in function of A is:

$$\sigma_{cr} = E\frac{\pi^2}{A^2}$$

Greater is the slenderness of the rod and lower is the critical load to send it in instability, so to avoid the deformation of the same at the same slenderness A, will be necessary to replace the constraints with wedging.
This treatment is valid for slender rods with A ≈ 55, while for stubby rods will use the expressions:

- Jhonson: $\sigma_{cr} = \sigma_s - \frac{\sigma_s^2 A^2}{4\pi^2 E}$ (σ_s yield strength)

- Tangent module: $\sigma_{cr} = \frac{\pi^2 E_t}{A^2}$

In which E_t is the elastic tangential modulus defined as the tangent of the angle that the linear stretch of the stress curve deformation of the material in the elastic field form with the abscissa, $E_t = tan\alpha$.

3.2.2. 2D Models

The models 2D are been used to analyze bidimensional element, considering negligible the size on which the body develops which is usually along the z axis and the other two dimensions x and y higher then z dimension. For the different structural models below describing, change the load condition used and consequently of internal tensions, with different characteristics in the deformation and so displacements of the analyzed element.

3.2.2.1. Shell

A shell structure consists of a thin-walled casing and if subjected to compression loads it goes into instability, so there are added stiffeners to withstand the distributed and concentrated loads.
This model is applied to panels with a size, thickness in general, negligible compared to other two. The panels resist to tangential tensions (τ) while the normal stresses are absorbed by the reinforcement elements.
The hypotheses of this method are:

- Between one cross element and the other, the geometry must not vary much (constant cross-section);
- The transversal loads are applied near the transversal stiffening elements;
- Normal loads are applied on longitudinal elements;

Assuming uniform normal stresses on the current and the constant transverse stresses on the panel:

$$q = \bar{\tau}\, s$$

Where q is the constant flow along all the panel, s the thickness of the panel and τ the tangential flow of stress.
Considering panel and current together with q absorbed by the panel and N the normal effort outgoing from the current, from the equilibrium on the currents result the following relation:

$$\frac{dN_x}{dx} = -q$$

From which results the normal stress N is linear to x (the direction of the current). Normal stresses are defined as:

$$\sigma = \frac{N}{A}$$

From which they are proportional to N and therefore linear on the current, but inversely proportional to the transverse area of the current.
Examined a single panel valued by constant flow q, the tangential force and the resulting moment on it are expressed as:

$$F = q\, L$$

$$M = 2\, q\, \Omega$$

The first equation shows that the tangential force on the panel is proportional to the flow on the panel and to the length of the panel.
The second relationship is defined as the first formula of Bredt that relates the resulting moment on the panel with the flow on the panel q and the area Ω formed between the deformed panel and the center of the osculating circle (that is the circle approximates to the curved panel).

If the panel is closed on itself, the overall force is zero but it has an infinite arm turns out to have a finite moment described by the first Bredt formula above, with resistance to torsion and resulting torsion gradient expressed as:

$$\dot{\theta} = \frac{q}{2G\Omega}\int \frac{dc}{s}$$

This equation is known as the second Bredt formula and relates the torsion gradient $\dot{\theta}$ with: the q-flow of the panel, the area Ω, the tangential module G, the circumference length of the panel closed on itself c and the thickness s of the panel.
If there are different panels in the cell, the expression is modified because the q streams are not constant and in the second Bredt formula q falls into the integral.

3.2.2.2. Plate

For the plate it is considered a geometry with two dimensions preeminent respect to the third one and if subjected to a stress it deforms stretching in the stress direction and shortening in the direction transverse to the stress, maintaining itself however always flat. Considering the equilibrium in an element of the plate on which the normal stress per unit of length act, multiply the forces by the length of the side on which they act and the following equations of equilibrium to the translation are obtained:

- Long x:

$$N_{x,x} + N_{xy,y} = 0$$

Where:

- $N_{x,x}$ is the normal stress to the face of the element which has per unit vector x and it is derived in relation with the x axis;

- $N_{xy,y}$ is the force acting on the face perpendicular to y and in the x direction, derived along the y-axis;

➢ Long y:

$$N_{xy,x} + N_{y,y} = 0$$

In which:

- $N_{xy,x}$ is the force acting on the face perpendicular to y and in the x-direction, derived along the x-axis;
- $N_{y,y}$ is the normal stress to the face of the element which has for unit vector y and is derived in relation to the y axis;

➢ Long z:

$$T_{x,x} + T_{y,y} + q_z = 0$$

Where:

- $T_{x,x}$ is the stress on the face perpendicular to the x-axis in z-direction, derived along the x-axis;
- $T_{y,y}$ is the stress on the face perpendicular to the y-axis in z-direction, derived along the y-axis;
- q_z is the stress on the face perpendicular to the z-axis in the z direction;

From the Cauchy theorem on the reciprocity of the shear stresses on the faces, the equilibrium to the rotation around the z axis is:

$$N_{xy} = N_{yx}$$

About the equations of equilibrium to the rotation in the plane result:

➢ Around y:

$$T_x = M_{x,x} + M_{xy,y}$$

- Around x:

$$T_y = M_{xy,x} + M_{y,y}$$

The other equation for solving the system comes from the equilibrium equations around y and x and the equation to the equilibrium long z-translation with the following expression:

$$M_{x,xx} + M_{y,yy} + 2 \cdot M_{xy,xy} + q_z = 0$$

Defined all the balances to the translation and rotation along the three axes, the system of equations is solved with resulting moments and forces applied to the plate.
Also, for the plate, as for the shell model described above, the stiffeners are applied for a greater resistance to loads and external stresses.
The plates work bit with transverse loads and to improve the resistance the panels are stiffed or are made sandwich plates with a heart that resists to the cut stresses and two faces that resist to bending.

3.2.2.3. Membrane

This model is used for thin-walled structures and uses the shape functions to relate displacements to external stresses.
Considering a point of the membrane with coordinates (x, y) the displacement field (u, v) are to be defined with the vector of the nodal degrees of freedom defined as:

$$\{q^{(e)}\}^T = [U_1\ V_1\ U_2\ V_2\ U_3\ V_3\ U_4\ V_4]$$

With an interpolating law the vector of unknown displacements is defined:

$$\{s^{(e)}\} = \begin{Bmatrix} u \\ v \end{Bmatrix} = [N^{(e)}]\{q^{(e)}\}$$

Where $\left[N^{(e)}\right]$ represents the array of shape or interpolating functions, and in general it is:

$$u = N_1U_1 + N_2U_2 + N_3U_3 + N_4U_4$$

$$v = N_1V_1 + N_2V_2 + N_3V_3 + N_4V_4$$

From which emerges that:

$$[N^{(e)}] = \begin{bmatrix} N_1\ 0\ N_2\ 0\ N_3\ 0\ N_4\ 0 \\ 0\ N_1\ 0\ N_2\ 0\ N_3\ 0\ N_4 \end{bmatrix}$$

Through the development in series the nodal displacements are:

$$\mathrm{u} = \alpha_0 + \alpha_1 x + \alpha_2 y + \alpha_3 xy$$

It is therefore necessary to write the coefficients α_i as a function of the nodal displacements U_i.
Assuming a rectangular element of unitary sides (height b and base a), introducing the normalized dimensionless coordinates:

$$\xi = \frac{x}{a}$$

$$\eta = \frac{y}{b}$$

The nodal displacements with normalized dimensionless coordinates are:

$$u = \alpha_0 + \alpha_1 a\xi + \alpha_2 b\eta + \alpha_3 ab\xi\eta$$

Inserting the coordinates relative to a node in this expression, the result is nodal displacements in the single node considered.

The shape functions in dimensionless coordinates have the following expression:

$$\begin{cases} N_1(\xi,\eta) = (1-\xi)(1-\eta) \\ N_2(\xi,\eta) = \xi(1-\eta) \\ N_3(\xi,\eta) = \xi\eta \\ N_4(\xi,\eta) = (1-\xi)\eta \end{cases}$$

With the peculiarity that the shape functions are 1 in the node relative to the function index and 0 in all the other nodes, also their sum is equal to the unit:

$$N_1 + N_2 + N_3 + N_4 = 1$$

Replacing the coordinates of the nodes in the displacements:

$$u(0,0) = \alpha_0 = U_1$$

$$u(1,0) = \alpha_0 + \alpha_1 a = U_2$$

$$u(0,1) = \alpha_0 + \alpha_2 b = U_4$$

$$u(1,1) = \alpha_0 + \alpha_1 a + \alpha_2 b + \alpha_3 ab = U_3$$

From which the displacements in the four coordinates of the rectangular element nodes are known.

3.2.3. 3D Models

The displacements and the dimensions of the element are not negligible compared to the axes and in this case both for the geometry and for the stresses and displacements, are considered the dependence on the three directions of the axes without approximations, this resulting the model more realistic than 2D and 1D. In FEM 3D analysis are selected the solids considering in its integrity the complete 3D geometry that is modeled as the overlap of 2D shell or beam 1D depending on the load condition considered.
Otherwise in 3D there are different problems because it is difficult to model, it is difficult to find errors and is more expensive in terms of computing time for the computer.
These models consider the variable stresses in the three axes directions, placing the nodes of the elements in space and not in the plane like the 2D and also the deformation and therefore the displacements are referred to the three main directions in the space depending on the directions of the axes.

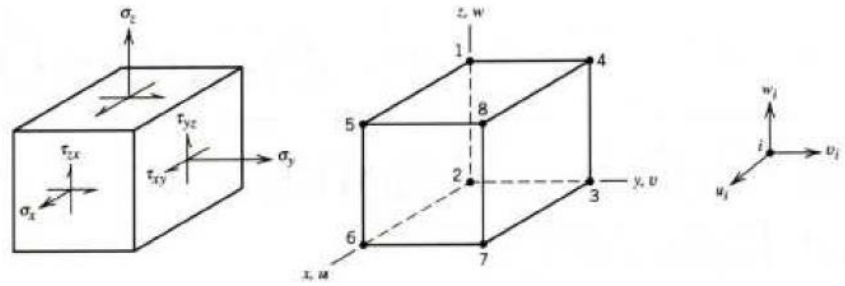

Figure 9-3D element representation

The global displacements of the element (s) can be related to the nodal displacements (q) by the shape functions (N):

$$\{s\} = [N]\{q\}$$

In which:

$$\{s\}^T = [u\ v\ w]$$

$$\{q\}^T = [U_1\ V_1\ W_1\ U_2\ V_2\ W_2\ U_3\ V_3\ W_3\ U_4\ V_4\ W_4]$$

$$[N] = \begin{bmatrix} N_1 & 0 & 0 & N_2 & 0 & 0 & N_3 & 0 & 0 & N_4 & 0 & 0 \\ 0 & N_1 & 0 & 0 & N_2 & 0 & 0 & N_3 & 0 & 0 & N_4 & 0 \\ 0 & 0 & N_1 & 0 & 0 & N_2 & 0 & 0 & N_3 & 0 & 0 & N_4 \end{bmatrix}$$

The sum of the N_i shape functions in the different nodes is equal to 1.
3D elements can be linear in parallelepiped, hexagonal or tetrahedral form.
In the studied cases the tetrahedral elements have been chosen because they better approximate the holes of the CAD models and for the implementation in the company software TADAP which uses these types of elements for thermodynamic reasons because they approximate better the aerothermal flow to atmosphere reentry.

Displacements along the three coordinates are:

$$u = \beta_0 + \beta_1 x + \beta_2 y + \beta_3 z$$

$$v = \beta_4 + \beta_5 x + \beta_6 y + \beta_7 z$$

$$w = \beta_8 + \beta_9 x + \beta_{10} y + \beta_{11} z$$

Where the coefficients β_i derive from the boundary conditions on the displacements in the nodes.
The resolution with the shape functions turns out to be the following:

$$N_i = \zeta_i = \frac{V_i}{V}$$

Where V_i is the displacement along the y-axis of the known i-node and V the displacement relative to the y-axis of the element. The three coordinates along the axes are written according to the shape functions like:

$$x = \sum_{i=1}^{4} x_i \zeta_i$$

$$y = \sum_{i=1}^{4} y_i \zeta_i$$

$$z = \sum_{i=1}^{4} z_i \zeta_i$$

Placing in nodes with dimensionless coordinates are obtained the displacements of the element.

3.3. Stiffness criteria

Stiffness criteria are intended to determine if the tensional state of a structural element is such as to lead to failure in terms of breakup or yield.

These criteria relate the critical material parameters, the strength or breakage stress of systems subjected to traction or compression, with the resistance of the element subjected to a biaxial or triaxial tensional state.

According to the experimental observation of the physical mechanism with which the material reaches a critical state, several theories have been developed that take the name of resistance criteria.

In general, the structures are designed for maximum stresses and they must be below critical stress defined as allowable stress, a fraction of the stress that causes the damage:

$$\sigma_a = \frac{\sigma_l}{n}$$

Where σ_l is the limit of stress to have a breakup or yield status and n the safety coefficient which by regulation is between $1.3 \leq n \leq 2$.

The safety coefficient "n" is imposed by legislation and according to the case chosen by the designer, to consider several factors:

- Uncertainty about the load and the applications (shocks, stresses for assembly or transport);
- Uncertainty about the properties of the material (inertial properties, variations for machining, wear and operating temperatures);
- Imprecision of the mathematical models (simplified theories);
- Additional stresses due to machining or assembly;
- Dangerous damage;
- Cost;

The criteria are distinguished for materials according to their characteristics:

- Ductile materials: high plastic deformation starting from the achieving of the yield stress σ_s inferior to that of break. Some criteria suggest the critical condition of ductile materials with the yield stress σ_s;

- Fragile materials: low plastic deformation and the critical condition in the stiffness criteria is that of breakup. Fragile materials have a higher compression resistance than traction, so there are two critical loads: the σ_{RT} tensile strength and the σ_{RC} compression breaking voltage.

The equivalent strain σ_e can be calculated with different stiffness criteria according to the material considered and must be less or equal to the permissible one, which depends on the experimental tests on the material, so that it doesn't break.
The materials according to their characteristics, isotropic or orthotropic, have different criteria to be referenced. For orthotropic materials:

- Maximum stress criterion: compares the stresses calculated with the resistance parameters of the material in the orthotropic reference.

$$-\frac{x_c}{\cos^2\theta} \leq \sigma_x \leq \frac{x_t}{\cos^2\theta}$$

$$-\frac{y_c}{\sin^2\theta} \leq \sigma_y \leq \frac{y_t}{\sin^2\theta}$$

$$|\sigma_S| \leq \frac{S}{\sin\theta\cos\theta}$$

It assumes as achieved a state of crisis if are verified the expressions of the system in which x_t is the tension limit of traction in x direction, x_c is the tension limit of compression in x direction, y_t is the tension limit of traction in the direction y , y_c is the compression limit voltage in the y direction, S the shear limit stress and θ is the angle of inclination of the fibers.

- Maximum deformation criterion: compares the deformation calculated with the resistance parameters of the material in the orthotropic reference.

$$-\frac{x_c}{\cos^2\theta - \nu_{12}\sin^2\theta} \leq \sigma_x \leq \frac{x_t}{\cos^2\theta - \nu_{12}\sin^2\theta}$$

$$-\frac{y_c}{\sin^2\theta - \nu_{21}\cos^2\theta} \leq \sigma_y \leq \frac{y_t}{\sin^2\theta - \nu_{21}\cos^2\theta}$$

$$|\sigma_S| \leq \frac{S}{\sin\theta\cos\theta}$$

The difference from the previous criterion lies in the addition of the Poisson coefficient ν_{12} because having composites that come to a fragile breakup, they are at the limit of the elastic tract and therefore do not vary the analysis for the shear verification while in the check for normal strain there is the Poisson coefficient.

- Tsai-Hill criterion: this criterion considers all the deformation energy or the distortion and the change of volume.

$$\left(\frac{\sigma_x}{x}\right)^2 + \left(\frac{\sigma_y}{y}\right)^2 - \frac{\sigma_x \sigma_y}{x^2} + \left(\frac{\sigma_S}{S}\right)^2 \leq 1$$

This expression is valid for an orthotropic foil in a tension plane state and it is a criterion that considers the interaction between the breaking mechanisms at the macroscopic level but does not determine the breaking mechanism and therefore the cause of the criticality, also there isn't distinction between tensile and compressive strength.

- Hoffmann criterion: this criterion is a generalization of the previous criterion of Tsai-Hill, but it distinguishes between tensile or compression strength.

$$\frac{\sigma_x}{x_t x_c}^2 + \frac{\sigma_y}{y_t y_c}^2 - \frac{\sigma_x \sigma_y}{x_t x_c} + \frac{x_c - x_t}{x_t x_c}\sigma_x + \frac{y_c - y_t}{y_t y_c}\sigma_y + \left(\frac{\sigma_S}{S}\right)^2 \leq 1$$

Hoffmann's criterion is simpler to be applied from the computational point of view compared to that of Tsai-Hill and in case of equal tensile and compression strength the two criteria coincide each other.

- Tsai-Wu criterion: this criterion compared to the others has additional resistance parameters compared to the previous criteria to better interpolate the experimental data.

$$\frac{\sigma_x}{x_t x_c}^2 + \frac{\sigma_y}{y_t y_c}^2 + 2F_{12}\frac{\sigma_x \sigma_y}{x_t x_c} + \frac{x_c - x_t}{x_t x_c}\sigma_x + \frac{y_c - y_t}{y_t y_c}\sigma_y + \left(\frac{\sigma_S}{S}\right)^2 \leq 1$$

Compared to the previous case is added in the equation of stresses the resistance tensor F_{12} defined as:

$$F_{12} = \frac{1}{2\sigma^2}\left[1 - \left(\frac{1}{x_t} + \frac{1}{x_c} + \frac{1}{y_t} + \frac{1}{y_c}\right)\sigma + \left(\frac{1}{x_t x_c} + \frac{1}{y_t y_c}\right)\sigma^2\right]$$

In which σ is the level of tension with which the biaxial breakup occurs and for $F_{12} = -\frac{1}{2}$ the Tsai-Wu criterion coincides with Hoffmann and if the tensile and compression resistance are equal it coincides with Tsai-Hill.

As far as isotropic materials are concerned, there are several criteria for describing the material breaking behaviour:

- Rankine-Navier criterion: also known as the maximum stress criterion, places the failure at the point where the main maximum stress agent on an element equals the yield stress of the material.

$$\sigma_e = \max\{\sigma_x, r\sigma_z\}$$

In this expression the equivalent stress σ_e to be compared with the admissible of the material, is the maximum stress in modulus between the major σ_x and the lesser σ_z multiplied by $r = \frac{\sigma_{lt}}{\sigma_{lc}}$ (ratio between the tensile and compression tension), considering only tensile or compression stress as possible causes of failure. This criterion is used in fragile materials by placing the breakup at the yield limit but does not consider the intermediate tensions between the maximum and the minimum.

- Tresca criterion: also known as the criterion of the maximum tangential tension, it states that the failure is made by yield when the maximum tangential tension at one point is equal to that of the tested specimen at the time of yield.

$$\sigma_e = \max\{|\sigma_x - \sigma_y|, |\sigma_x - \sigma_z|, |\sigma_y - \sigma_z|\}$$

From which the equivalent stress σ_e is taken, to be compared with the admissible one, which is equal to the maximum modulus of the difference of the applied stress to the element, along the three main axes. This criterion considers only the maximum and minimum voltage, neglecting the intermediates, and applies to ductile materials. It is not

possible to use it in the plastic field because the material has different behavior according to the applied stresses.

- Octahedral tensor criterion: this criterion considers tangential and normal stresses on four octahedral planes that form with the main axes equal angles of 54.74 degrees.

$$\sigma_e = \frac{1}{\sqrt{2}}\sqrt{\left(\sigma_x - \sigma_y\right)^2 + \left(\sigma_y - \sigma_z\right)^2 + (\sigma_x - \sigma_z)^2}$$

The resultant equivalent strain of the preceding expression should be compared with the permissible material and states that yield in ductile materials occurs when the octahedral voltage reaches the critical value.

- Coulomb-Mohr criterion: considers the material crisis in the plane in which there is a critical combination of tangential and normal strains that describe in the Mohr plane some circles, whose tangents indicate the limit to traction or compression.

$$\sigma_e = \max\{\sigma_x, r\sigma_z, \sigma_x + r\sigma_z\}$$

From the previous relation the equivalent stress is obtained to compare with the admissible stress where the main tensions are ordered as $\sigma_x > \sigma_y > \sigma_z$ and $r = \frac{\sigma_{lt}}{\sigma_{lc}}$.

3.3.1. Von Mises-Hencky criterion

Among all the resistance criteria usable, Von Mises criterion was chosen because in the analyses studied are considered isotropic materials and it is also the most complete since it considers normal and tangential tensions in the expression of the equivalent stress with a low computational cost. This criterion is also defined as the criterion of the distortion

energy because it states that the yield is when the elastic deformation energy reaches a critical value, determined like the deformation energy relative to the monoaxial yield strain. Being the Von Mises criterion based on elastic field sizes, it can be used to identify only the strain combinations that cause yield (combinations that represent the upper limit in elastic field).

This criterion considers that ductile materials subject to the main compression strain of equal values cause a variation in volume and not in form with higher yield strength than the value of tensile tests.

To have the Von Mises criterion, the distortion work of U_d is determined as the difference between the total work U and the one that causes variation of volume U_v comparing it with the one relative to the simple traction.

For the evaluation of the distortion work perform the following steps:

- Evaluation of total deformation work U;
- Calculation of the average strain σ_m agent and work accomplished by it U_v;
- Distortion work as a difference $U_d=U-U_x$;

The work of the main strains is defined as:

$$U_i = \frac{\epsilon_i \sigma_i}{2}$$

Replacing ϵ with Hooke's law, the total deformation energy in the main directions is:

$$U = U_x + U_y + U_z = \frac{1}{2E}[\sigma_x^2 + \sigma_y^2 + \sigma_z^2 - 2\nu(\sigma_x\sigma_y + \sigma_x\sigma_z + \sigma_y\sigma_z)]$$

The deformation energy due to the variation in volume is obtained by substituting in place of the three main stains, the average strain component obtaining is:

$$U_v = \frac{1-2\nu}{6E}[\sigma_x^2 + \sigma_y^2 + \sigma_z^2 + 2(\sigma_x\sigma_y + \sigma_x\sigma_z + \sigma_y\sigma_z)]$$

From the difference between the total energy and the volume variation results the distortion energy:

$$U_d = U - U_v = \frac{1+\nu}{3E}[\sigma_x^2 + \sigma_y^2 + \sigma_z^2 - (\sigma_x\sigma_y + \sigma_x\sigma_z + \sigma_y\sigma_z)]$$

In case of tensile test at yield strength $\sigma_x=\sigma_s$ e $\sigma_x=\sigma_y=0$ with the resultant distortion energy equal to:

$$U_d = \frac{1+\nu}{3E}\ \sigma_s$$

From which the limit condition to yield is:

$$\sigma_s = \sqrt{\sigma_x^2 + \sigma_y^2 + \sigma_z^2 - (\sigma_x\sigma_y + \sigma_x\sigma_z + \sigma_y\sigma_z)}$$

From the previous equation of stress at yield field is obtained the equivalent tension of Von Mises for a system with not main axes and it is:

$$\sigma_e = \sqrt{\sigma_x^2 + \sigma_y^2 + \sigma_z^2 - \left(\sigma_x\sigma_y + \sigma_x\sigma_z + \sigma_y\sigma_z\right) + 3(\tau_{xy}^2 + \tau_{yz}^2 + \tau_{zx}^2)}$$

Defined as the equivalent stress of Von Mises, it should be compared with the admissible stress of the material which is the limit case for break status.

4. Study cases

In this project it has been chosen to analyse different components to the destructive re-entry in the atmosphere: a bench made of ceramic material, a washer of a demisable joint of the Sentinel-1 satellite and an assembly of joint that connect the external panels of the satellite Sentinel-1.

4.1. Bench

In this project the first component analysed was the bench whose dimensions and properties are very closed to the one analysed in the context of project lead by TASinI in Turin called D4OP (Demisability For Optical Payload).
The bench has been analysed for its peculiarity of being a component made in ceramic material and resists to high temperatures, therefore difficult to demise when re-entering in atmosphere. It is important to consider that the bench is inside the satellite and so it is not exposed to the thermal flow of re-entry until the outer panels of the satellite are detached and therefore is completely exposed to the external conditions of re-entry.
Eventually the optical benches are very interesting for destructive re-entry since they can fragment due to structural loads, resulting in different impacting fragments. These fragments cannot be identified by current re-entry tools (which only focus on aerothermodynamic demise), finally underestimating casualty risk w.r.t. reality.
The bench geometry is the following with dimensions expressed in millimeters and the thickness is 9.35 mm.

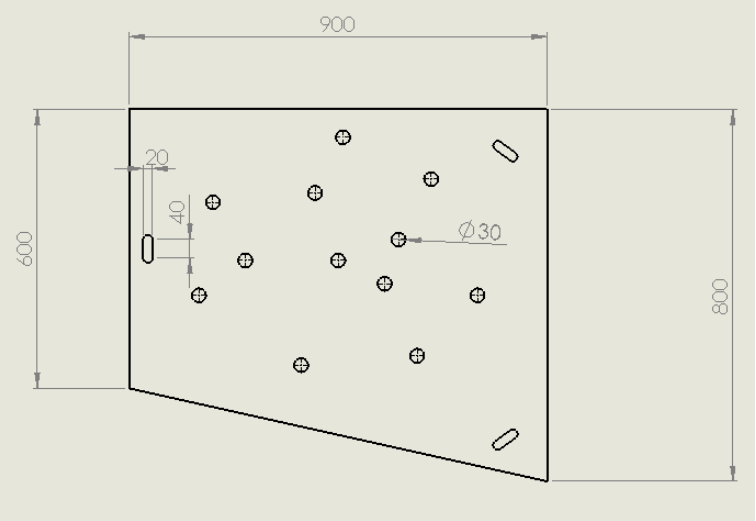

Figure 10-Bench geometry in mm

4.1.1. Input properties and loads

Regarding the properties of the material, the bench is composed in Si3N4 (Silicon Nitrate) a ceramic material that resists at very high temperatures as possible to see from the thermal expansion coefficient. Being a ceramic material, even if it has the elastic modulus and the resistance to breakage that decreases with the temperatures, the Poisson coefficient and density don't change substantially and even for the temperature range represented, they turn out to be constant.

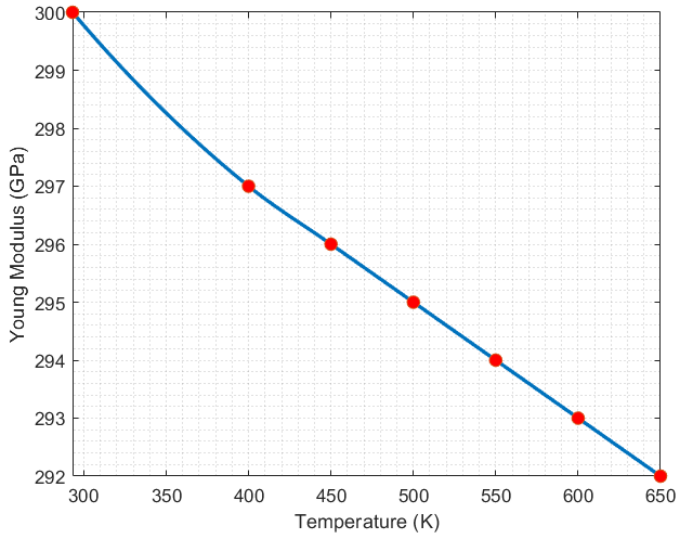

Figure 11-Elastic modulus of silicon nitrate vs temperature

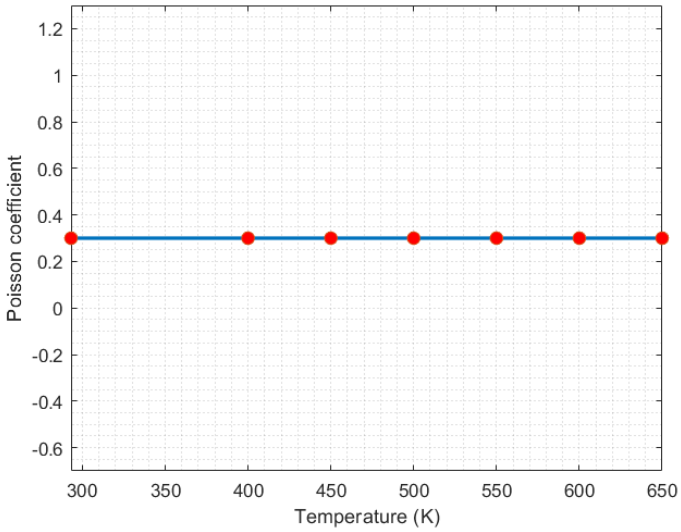

Figure 12-Poisson coefficient of silicon nitrate vs temperature

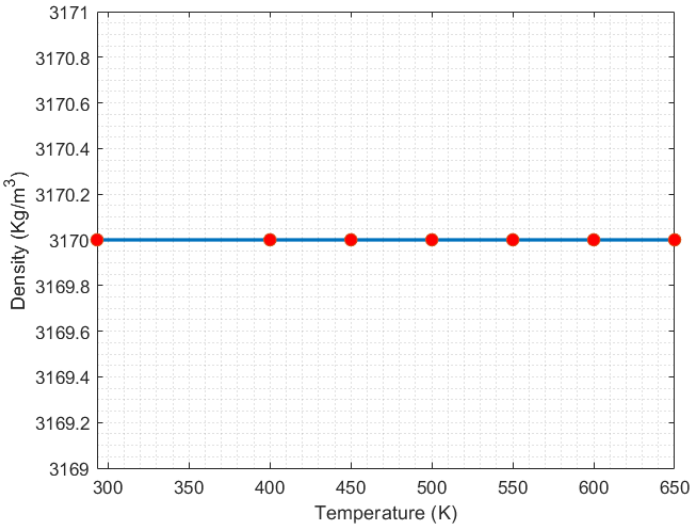

Figure 13- Density of silicon nitrate vs temperature

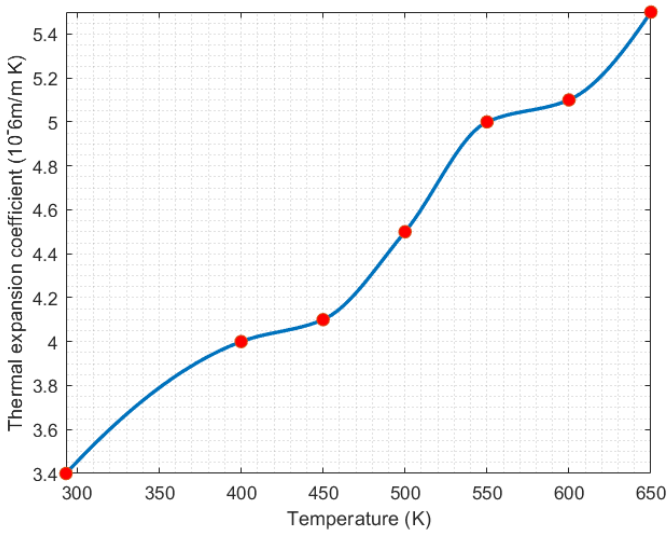

Figure 14- Thermal expansion coefficient of silicon nitrate vs temperature

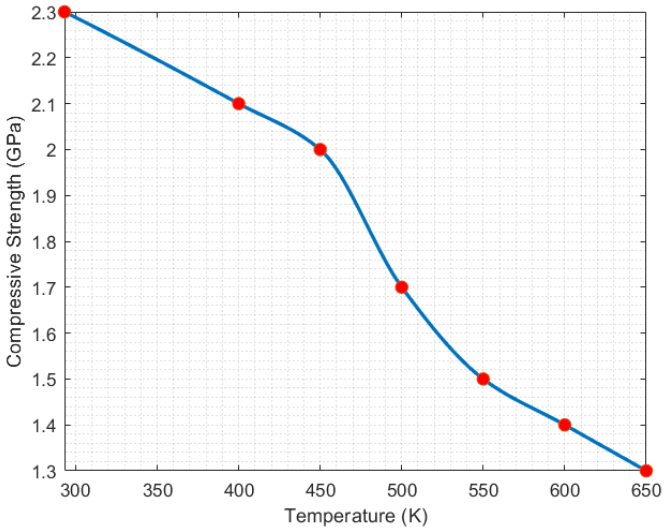

Figure 15-Compressive strength of silicon nitrate vs temperature

The defined properties of the material vs the temperature, were applied in the FEM simulations performed with PATRAN for the unless otherwise conditions considered to re-entry, referring to an average temperature of the bench.

Regarding the loads imposed on the bench, different nodal temperatures between the central, intermediate and external zone, are been imposed and they go gradually to increase from the inside to the outside zone for the different exposure to the thermal flow. To give an idea of the thermal loads applied are reported below the three different zone in which there are three different temperatures.

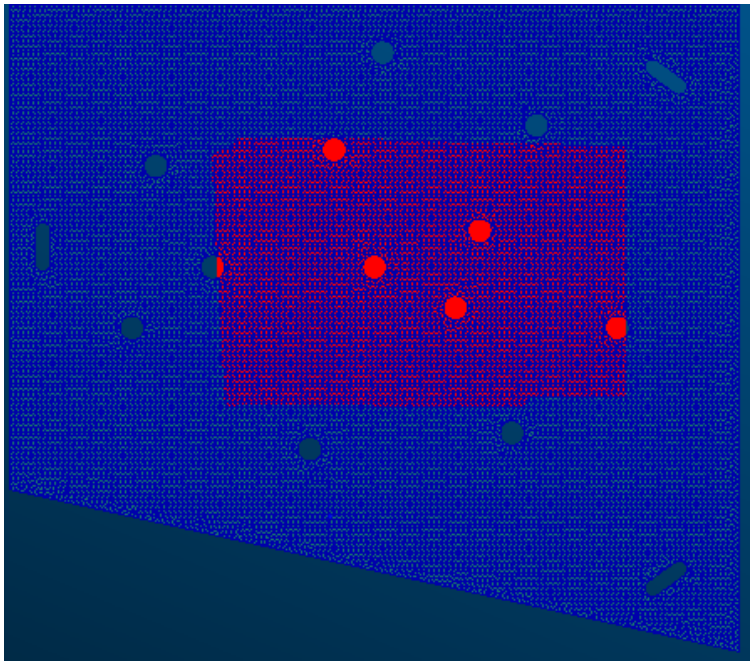

Figure 16-Central zone temperatures

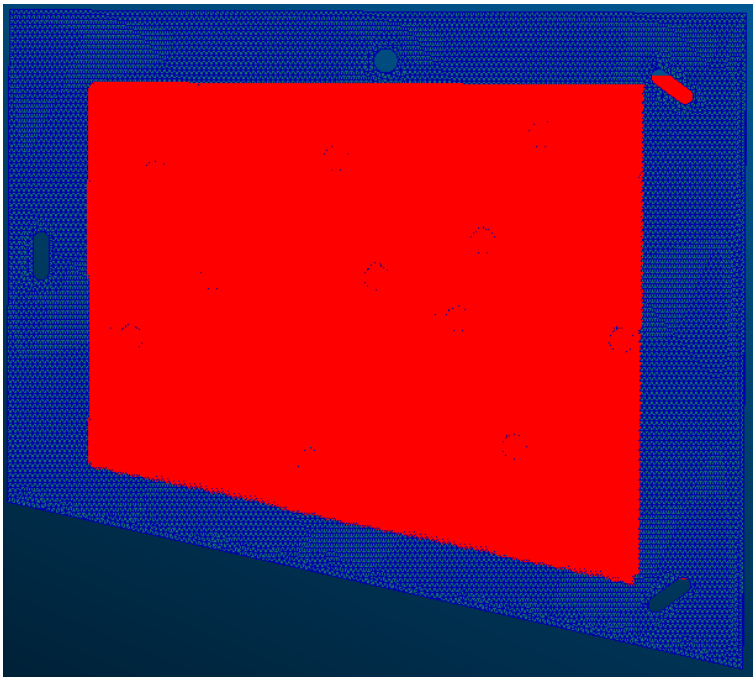

Figure 17- Intermediate and central zone temperatures

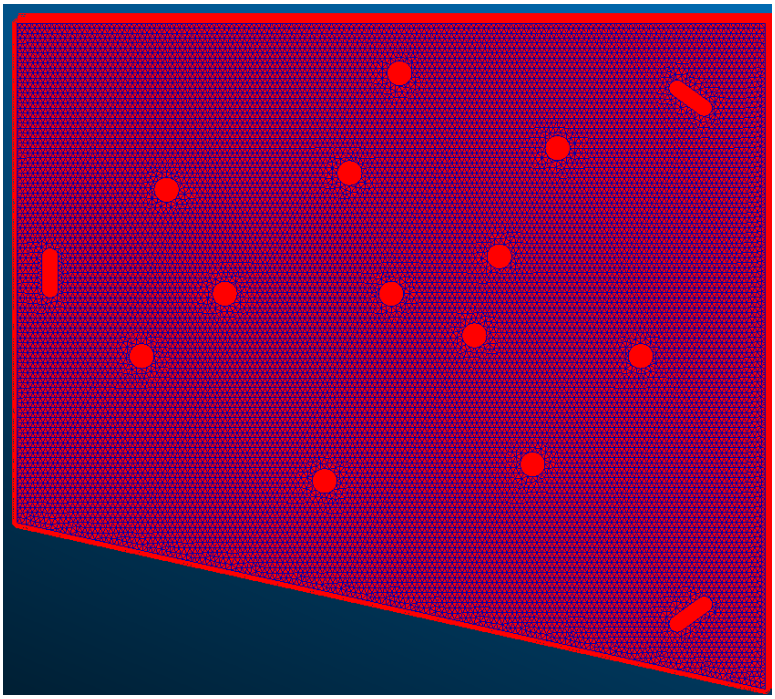

Figure 18- External, Intermediate and central zone temperatures

In addition, there are inertial loads due to the linear accelerations that increase exponentially after the 85 km and at the angular velocities of the satellite in the tumbling phase that occur after 90 km and under-represented in the graphic. They are set in Patran with inertial loads card to entire model without selecting any region. These data come from the analyses did in the context of D4OP study.

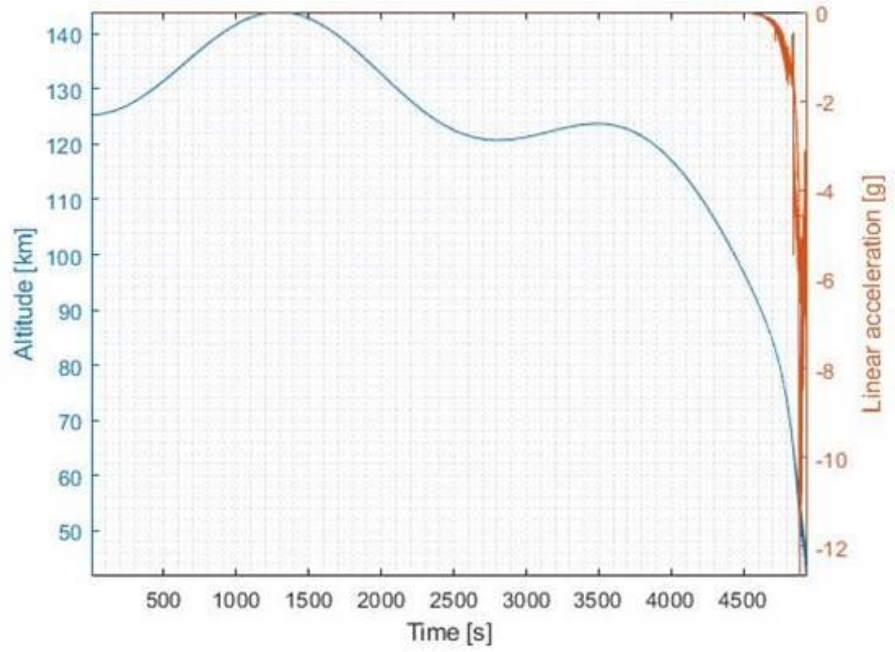

Figure 19-Linear acceleration on the Bench

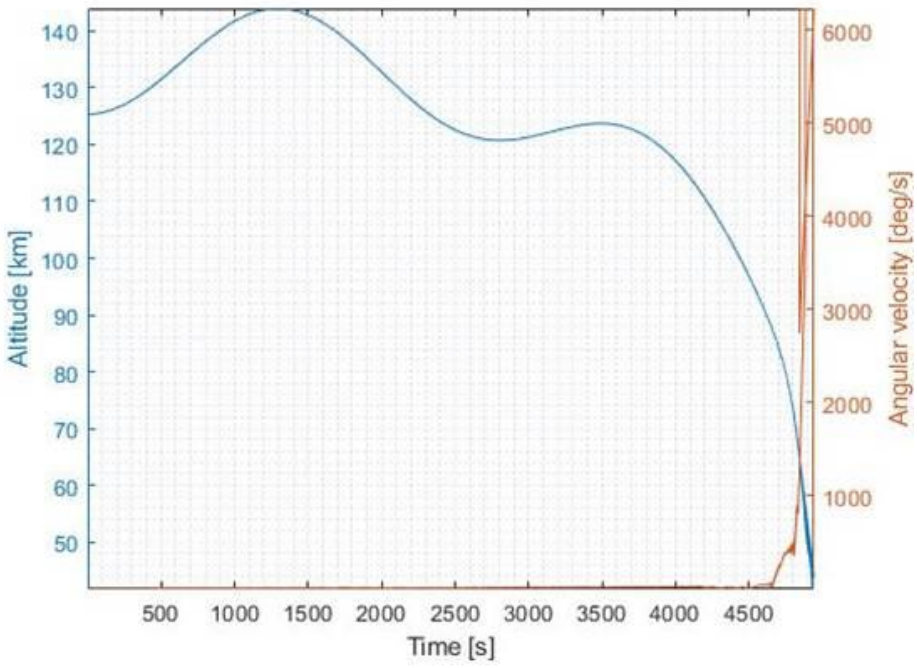

Figure 20-Angular Velocity on the Bench

For what concerns the constraints, on the bench have been applied wedging constraints on the nodes of the slots locking the translations and rotations along the main axes.

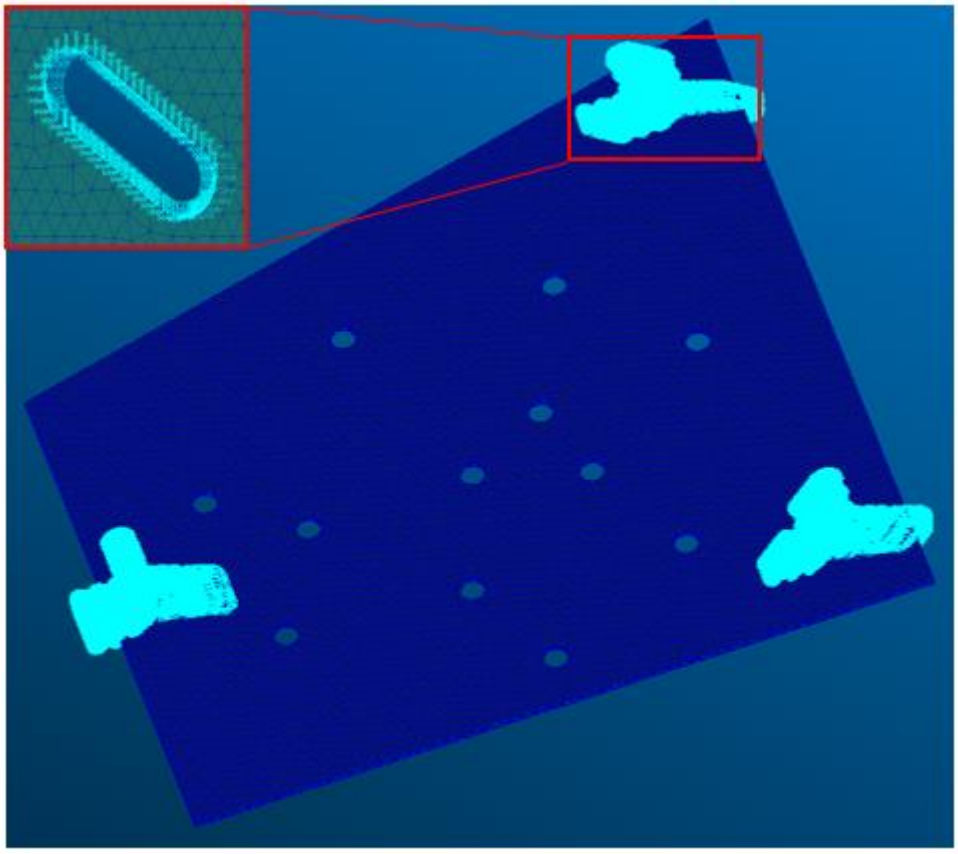

Figure 21-Constraints representation for the bench

4.1.2. Mesh convergence

To evaluate results, a preliminary mesh convergence analysis was made in which thermal loads were imposed at 500 K in the bench knots and inertial loads of 1 g on the mesh elements.

Regardings the constraints, have been imposed wedging constraints in the knot of the slots, like illustrated in Figure 21, and analyzed in the four free vertices of the bench displacements and Von Mises tensor, numbered from 1 to 4 anticlockwise starting from the lower left, referring to the above geometry.

To understand how the mesh density changes in this analysis, two figures with lowest and highest number of nodes are been reported below.

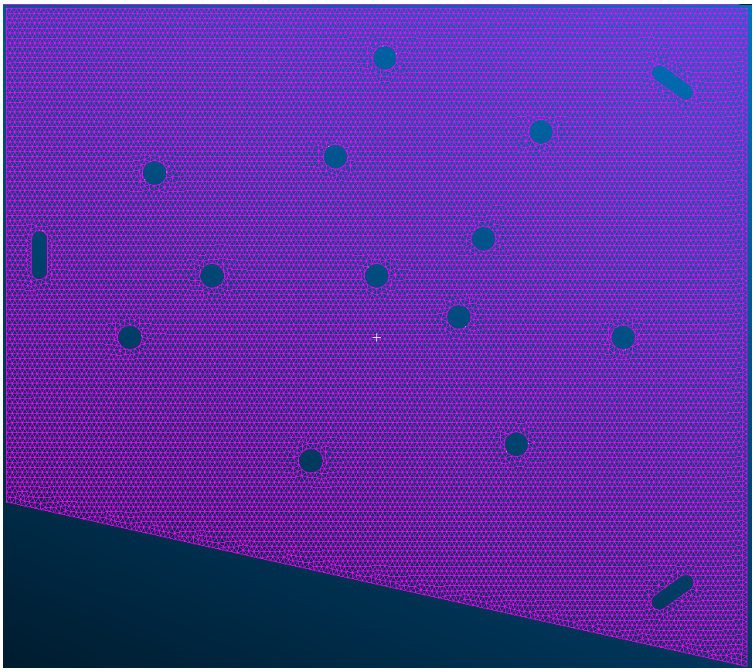

Figure 22-Mesh with about 300000 nodes

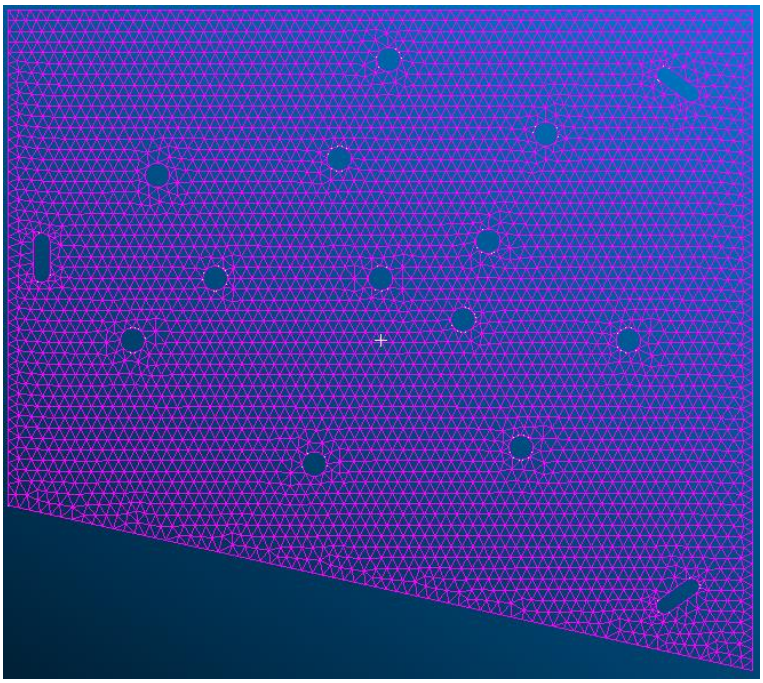

Figure 23- Mesh with about 50000 nodes

4.1.2.1. 2D Mesh convergence

For mesh convergence analysis with 2D elements, were used bidimensional square elements QUAD8, with 8 nodes for each mesh element, and a thickness of 9.35 mm was set for each element to reflect the real size of the bench.

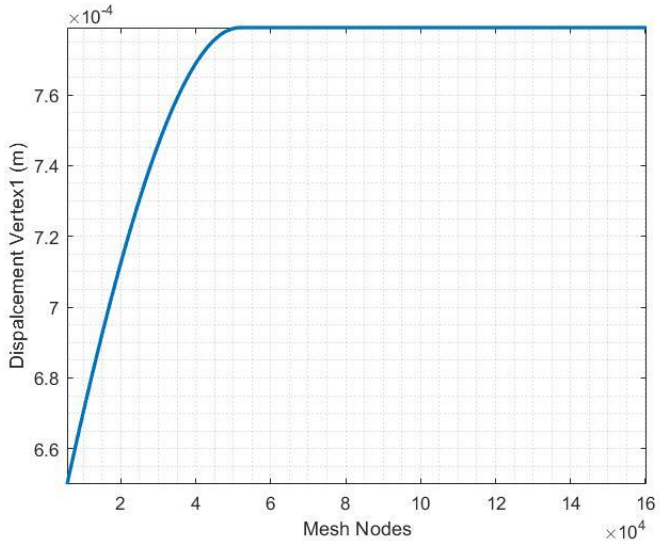

Figure 24-Displacement vertex 1 vs mesh nodes

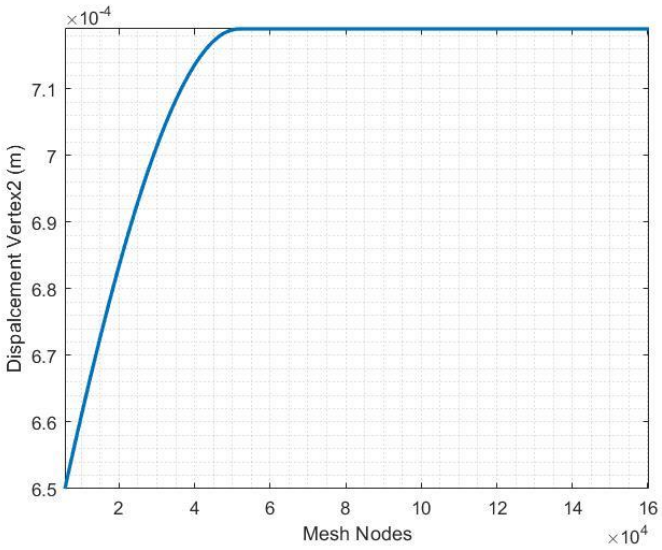

Figure 25- Displacement vertex 2 vs mesh nodes

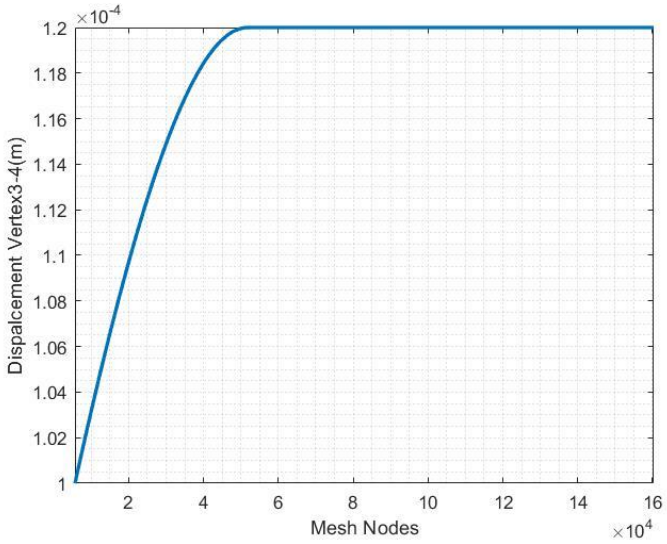

Figure 26- Displacement vertex 3-4 vs mesh nodes

The analyses carried out and the results above reported show that the displacements increase as the mesh nodes increase. The displacements increase to an asymptotic value in which the mesh density, for the geometry considered, has a correct value to describe real behaviour of the component in fact increasing mesh nodes, the displacements remain constant. For the analysis of the real model are used the minimum number of nodes to convergence occurred on the displacements of the vertices, to have a low computational cost and to obtain the results of the analyses in the shortest time possible.

A visualization of the indicative results on the displacement map and the tensor of Von Mises are the ones shown below.

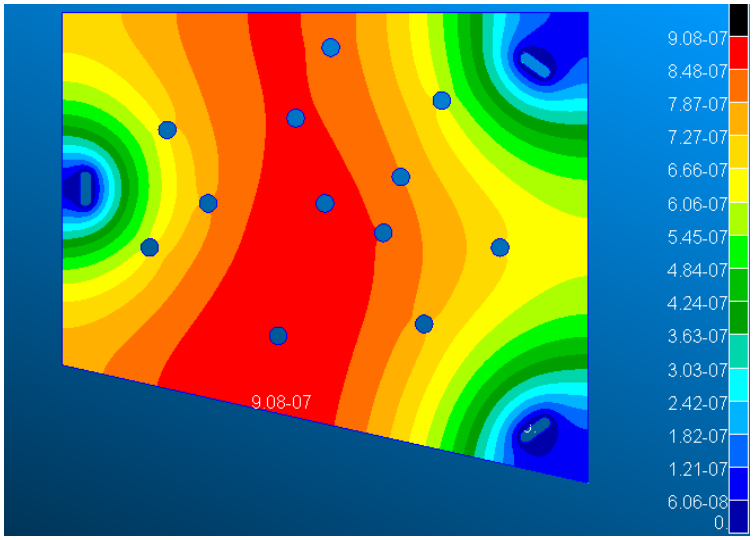

Figure 27-2D Displacement map (m) of the 3.35 mm thick bench

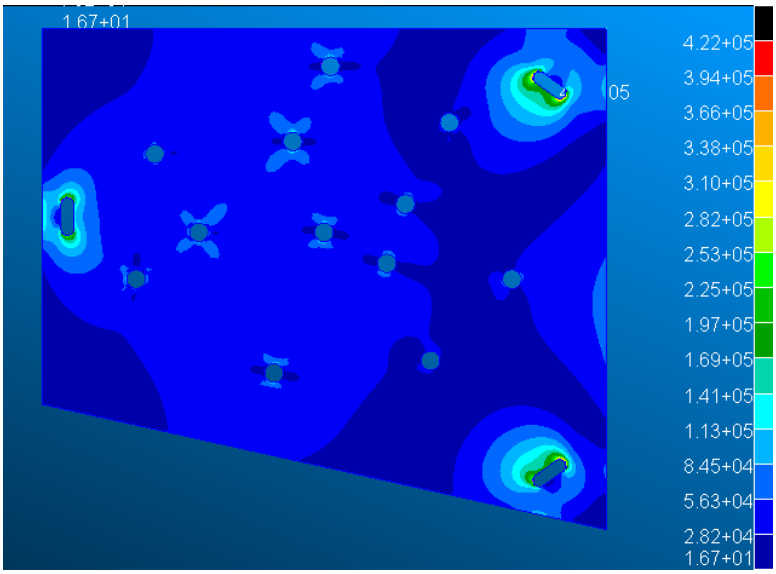

Figure 28-2D VM Stress map (Pa) of the 3.35 mm thick bench

The displacement map show that the maximum value is found in the central area of the bench, having an inertial load that acts in the center of gravity mainly and the maximum of stress is detected near the slots in which it is fixed and where cracks likely develop.

4.1.2.2. 3D Mesh convergence

For the analysis of mesh convergence with 3D elements, three-dimensional tetragonal elements were used TRIA10, with 10 knots for each 3D mesh element, and was considered the solid of the bench with a thickness of 9.35 mm to reflect the real size of the bench.

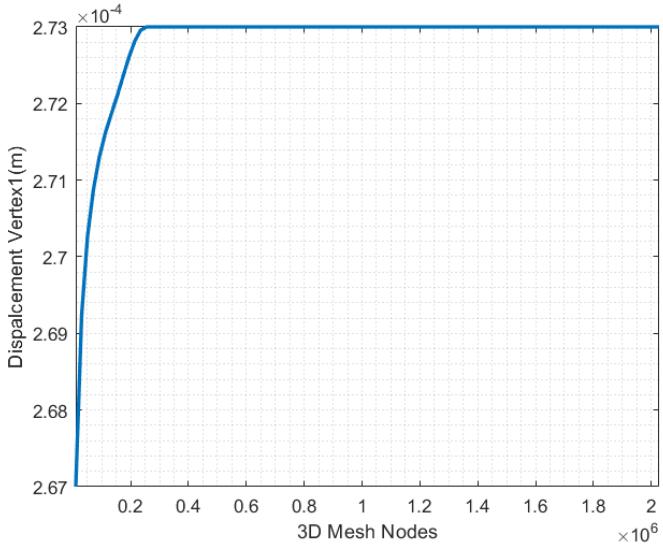

Figure 29- Displacement vertex 1 vs mesh nodes

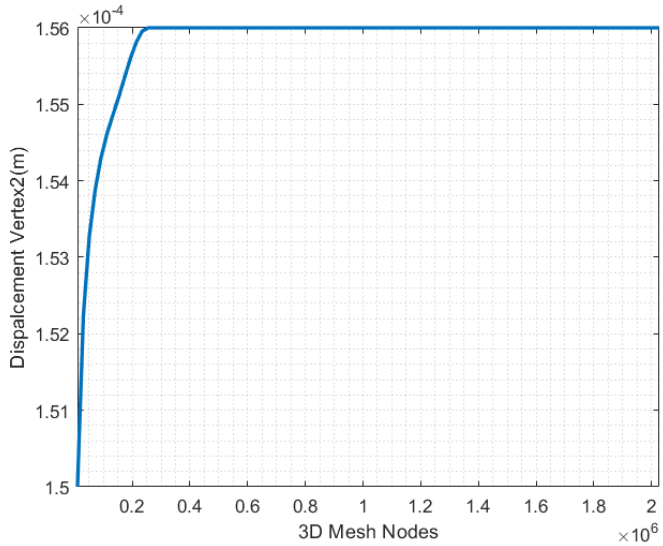

Figure 30- Displacement vertex 2 vs mesh nodes

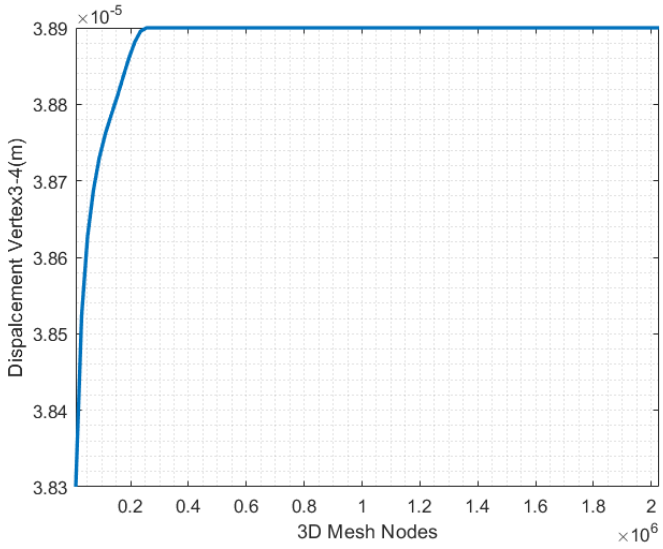

Figure 31- Displacement vertex 3-4 vs mesh nodes

From the analyses carried out with a 3D mesh and the results upper shown, the displacements increase as the mesh nodes increase up to an asymptotic value for the same motivation described above for the 2D. For the analysis of the real model are been used the minimum number of nodes to convergence occurred on the vertices displacements to have a low computational cost and to obtain the results of the analyses in the shortest time possible.

A representation of the indicative results is reported on the displacement map and Von Mises tensor that are shown below.

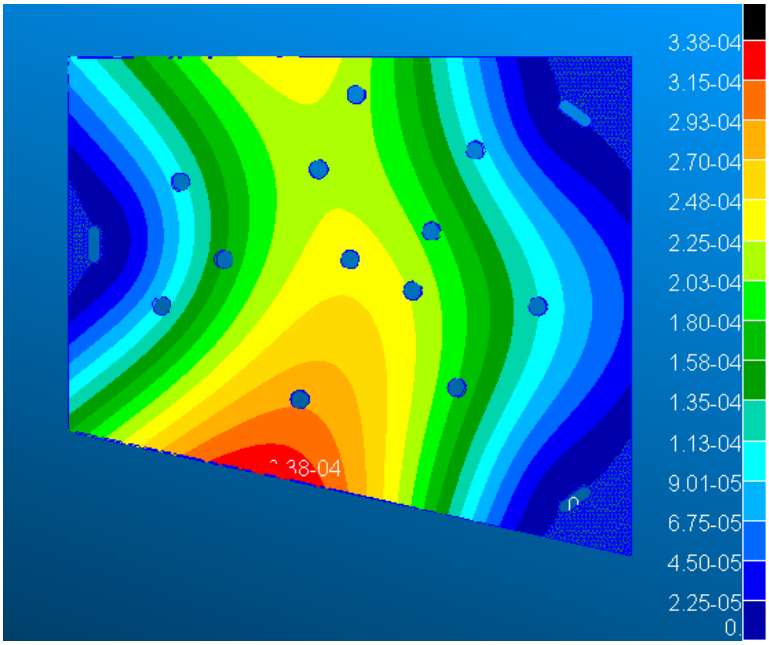

Figure 32-3D Displacement map (m) of the 12.35 mm thick bench

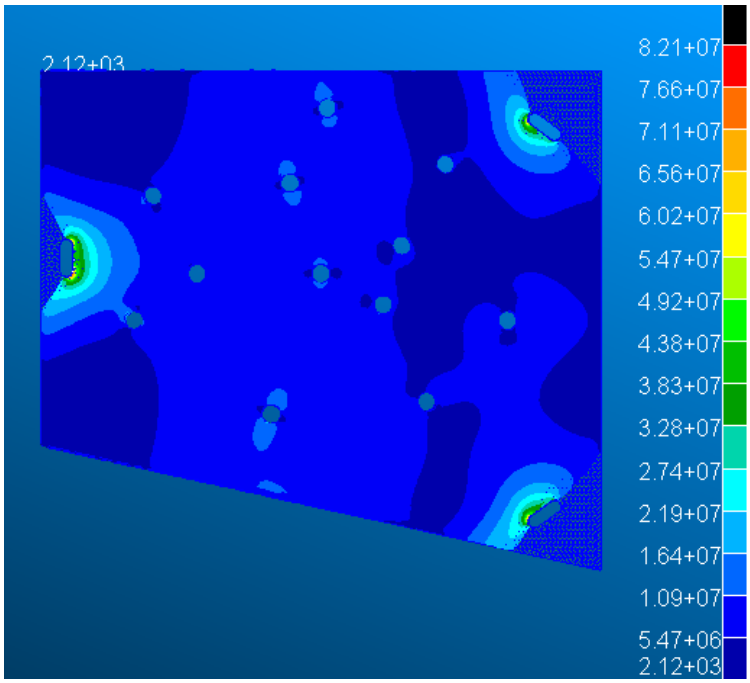

Figure 33-3D VM Stress map (Pa) of the 12.35 mm thick bench

As for the 2D, even for the 3D, the displacement map show that the peak is in the central area of the bench having an inertial load that acts in the centre of gravity mainly while the peak of the stress is detected near the slots in which it is fixed and cracks.

4.1.2.3. Comparison mesh 2D-3D

Setting the minimum of nodes for which convergence is achieved, a further convergence analysis has been performed between 2D and 3D meshes by examining the displacements and the tensor of Von Mises of the four vertices at the ends of the bench vs the thickness.

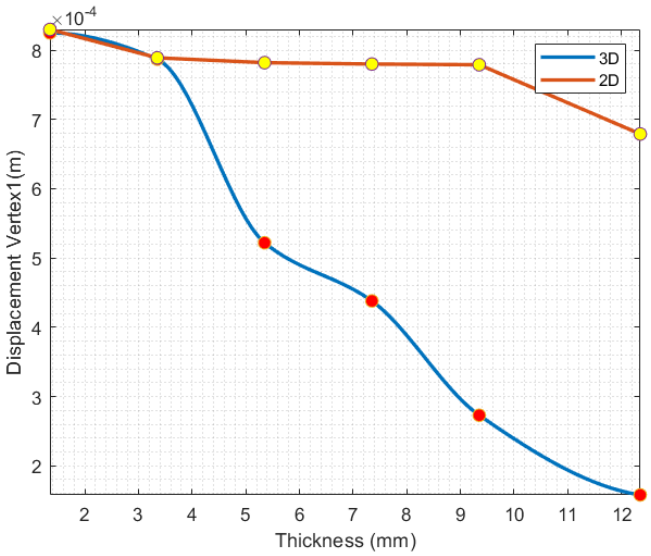

Figure 34- 2D&3D Displacement vertex 1 vs thickness

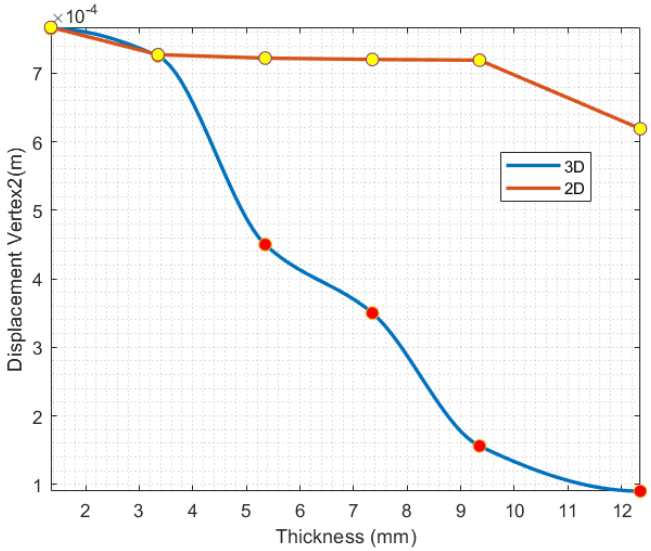

Figure 35-2D&3D Displacement vertex 2 vs thickness

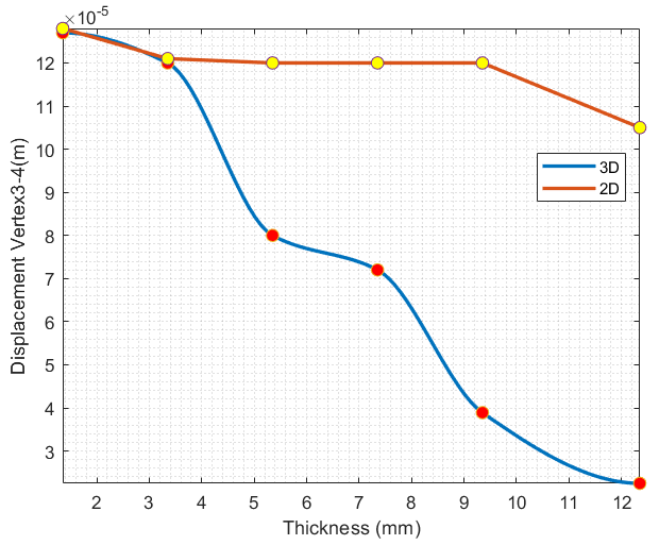

Figure 36-2D&3D Displacement vertex 3-4 vs thickness

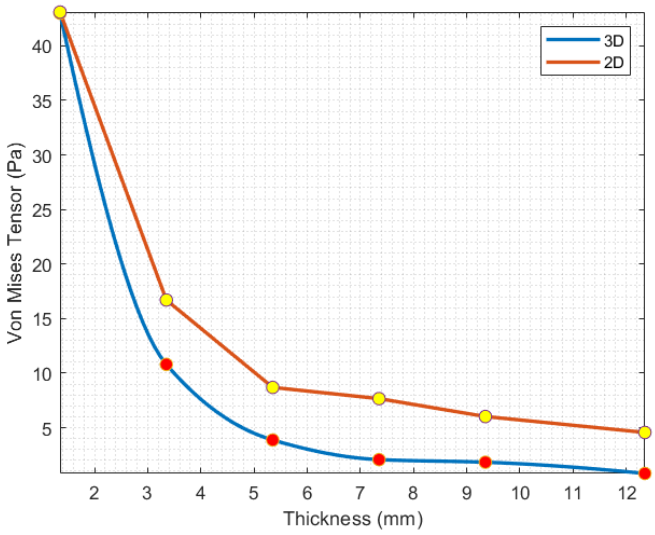

Figure 37-2D&3D Von Mises Tensor of vertices vs thickness

Comparing 2D and 3D mesh convergence can be seen that the decrease of the thickness of the bench brings displacements and stresses gradually to coincide with each other to confirm the correct convergence of the mesh and the difference between 2D and 3D.
To have less possible approximations and for a more realistic model in the simulation of the real bench, tetragonal 3D elements were used.

4.1.3. Results

From the considerations and analyses carried out for the convergence of the mesh show that the minimum number of nodes to which it has convergence and therefore to be used is about $3 \cdot 10^5$ knots.

By setting the analysis with loads and properties depending on altitude and on temperature, set differently in three zones of the bench (central, intermediate and external), the results are below in terms of displacements and stresses.

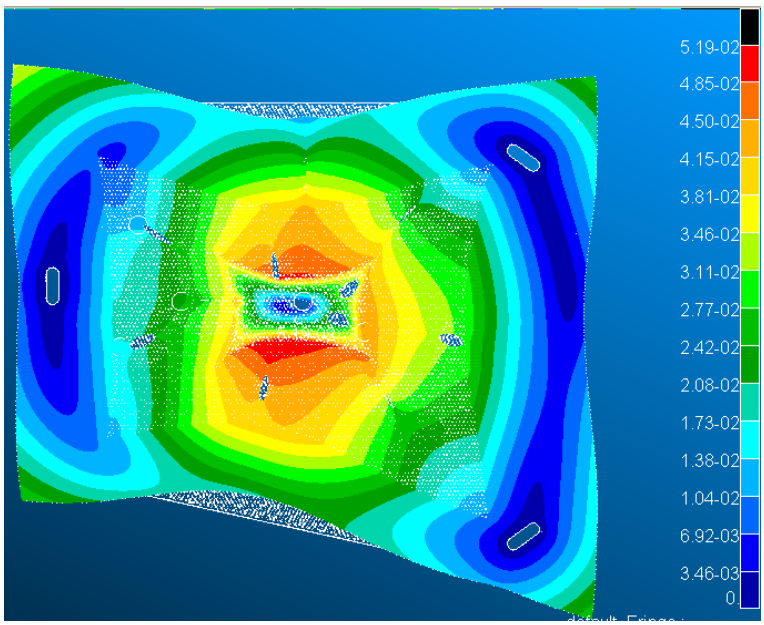

Figure 38- Displacement (mm) representation of the 9.35 mm thick bench at 90 km

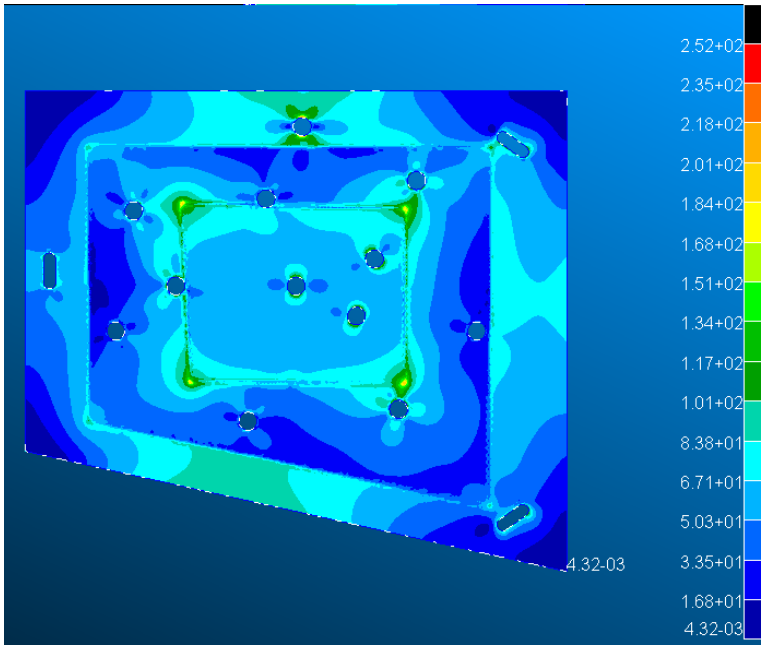

Figure 39- VM tensor (MPa) map of the 9.35 mm thick bench at 90 km

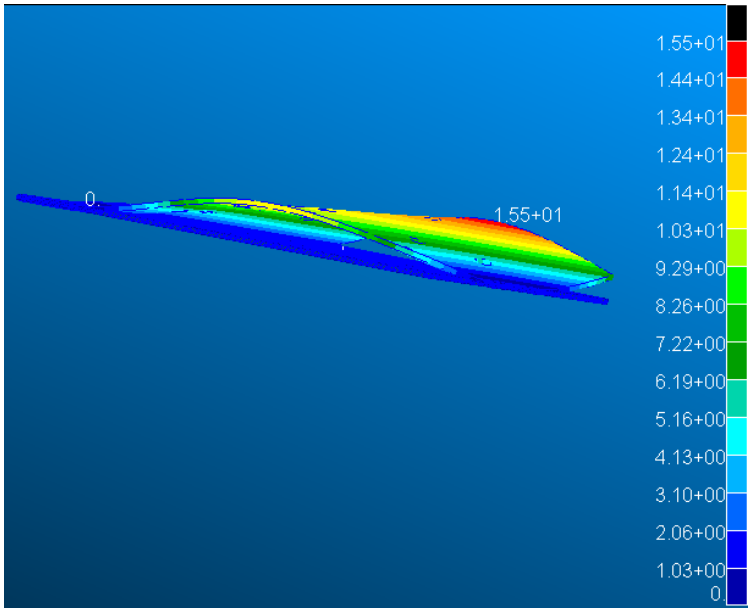

Figure 40-Displacement (mm) representation of the 9.35 mm thick bench at 80 km

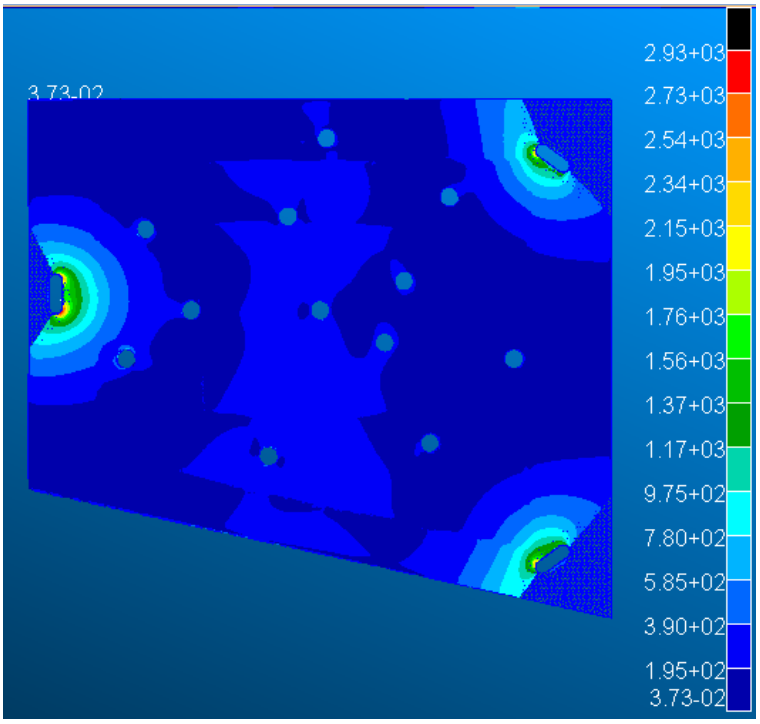

Figure 41-VM tensor (MPa) map of the 9.35 mm thick bench at 80 km

The figures above represent displacements and stresses on the bench at 80 km and 90 km with a maximum stress of 2930 MPa at 80 km which is much higher than its resistance limit of 2000 MPa referred to an average temperature (450 K) of the bench at 80km and the FEM analyses performed that it breaks between 90 and 80 km.

4.2. Washer

The second study case analysed is the washer that is part of a project of TASinI in Turin concerning the demisable Joint used to hold together the external panels of the satellite ever and was used on Sentinel-1. The peculiarity of this joint is the washer that is made in a zinc-based alloy named EZAC, it melts at ca 400 °C, a quite low melting point, so that it has the chance of demising at ca 90km of altitude inducing a separation of the joint and then of the external panels of the S/C, eventually increasing the external flux on the inner components, reducing the possibility some fragments can hit the ground.

Unlike the bench, the washer is a component of easy demisability for the metallic material of which it is composed and for the eternal position to the satellite it is exposed entirely to the thermal flow to re-entry to the atmosphere.
The geometry of the washer is as it follows with the dimensions in millimetres, a rounding of 1mm at 45° and the thickness of 2 mm.

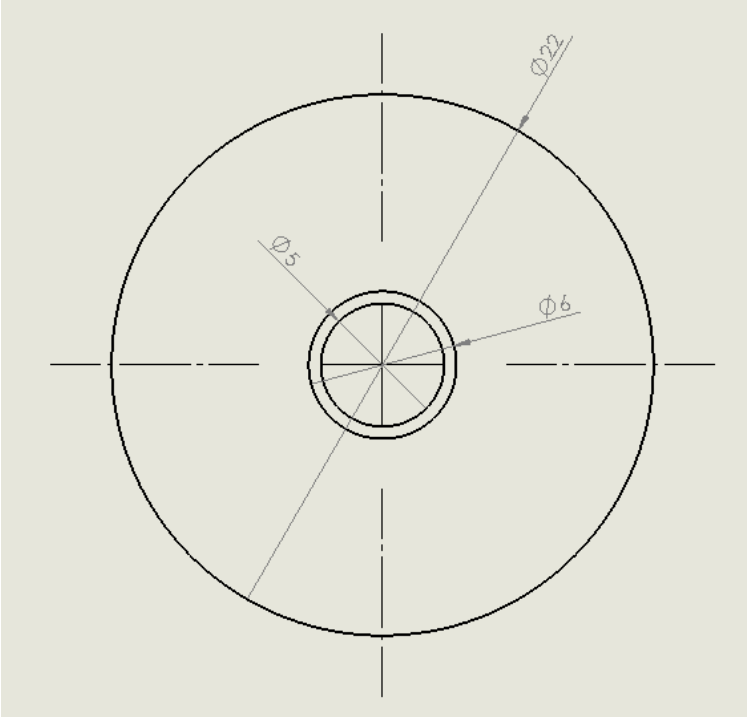

Figure 42-Washer geometry in mm

4.2.1. Input properties

Regarding to properties of the material, the washer is made in EZAC a zinc alloy that is easy to demise as noted by the coefficient of thermal expansion that is higher than the same of Si3N4, a ceramic material, and therefore expands more than a ceramic material when exposed to the thermal flux of the reentry.
As the temperature rises, the properties of the material decrease all but not the coefficient of thermal expansion, because since the temperature increases the expansion of the component increases.

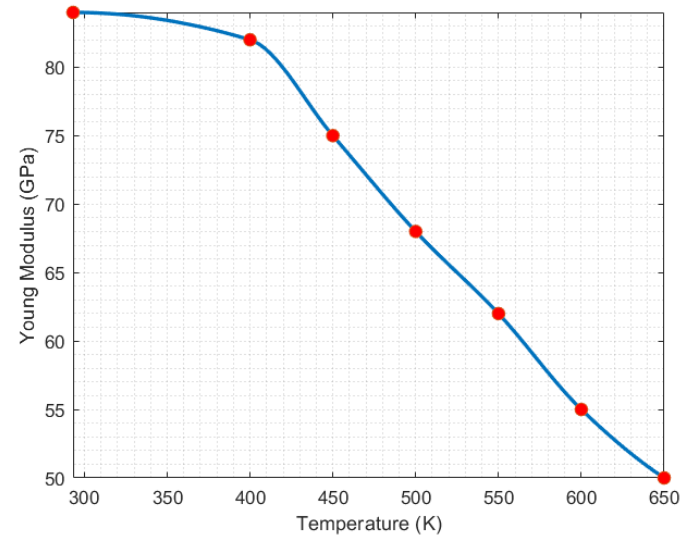

Figure 43- Elastic modulus of EZAC vs temperature

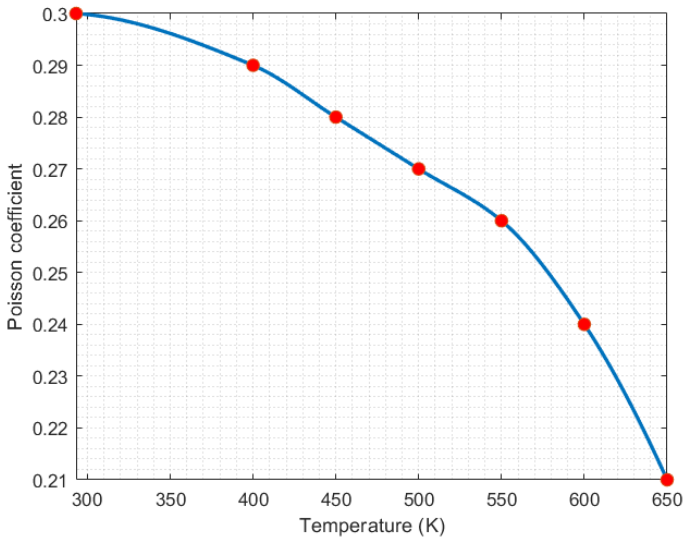

Figure 44- Poisson coefficient of EZAC vs temperature

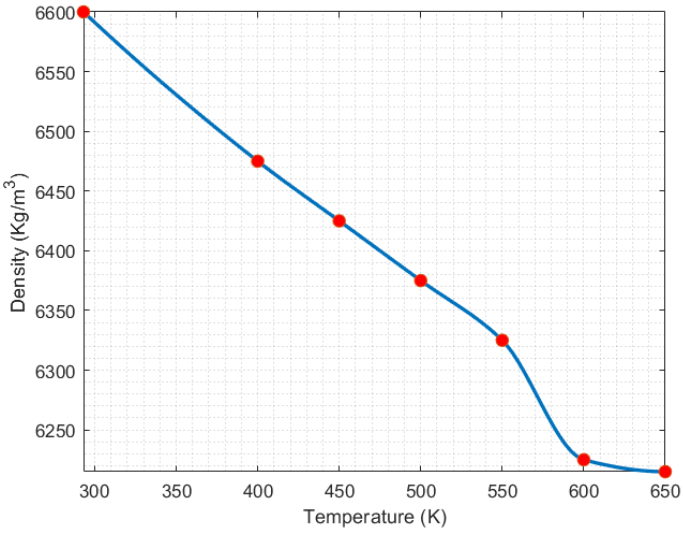

Figure 45- Density of EZAC vs temperature

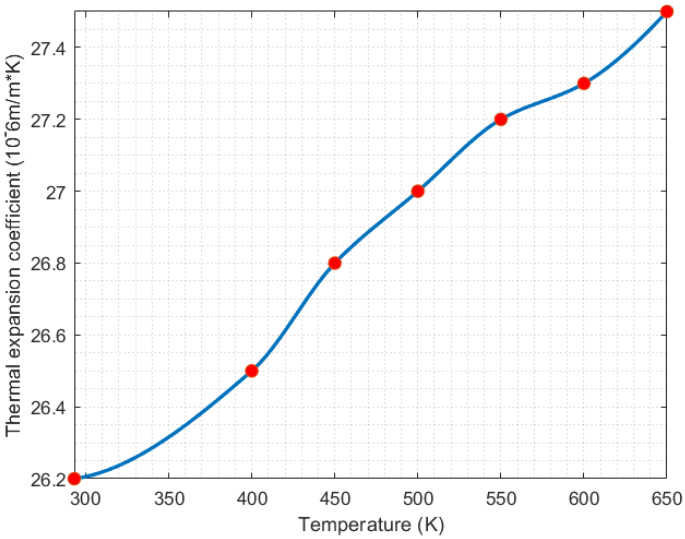

Figure 46- Thermal expansion coefficient of EZAC vs temperature

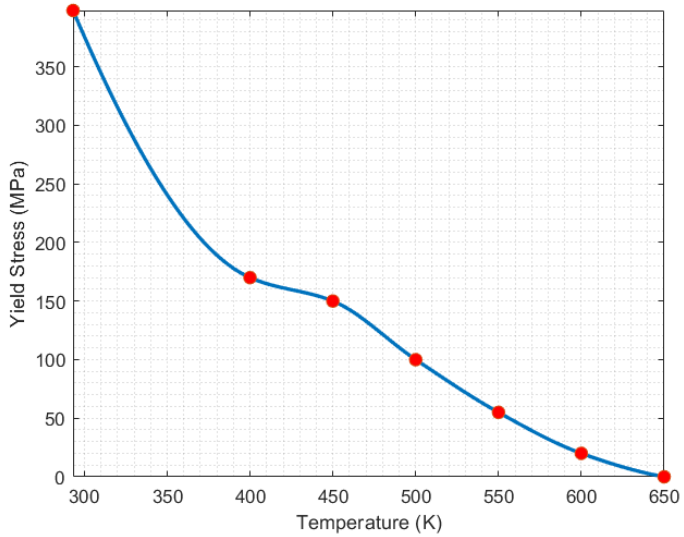

Figure 47- Yield stress of EZAC vs temperature

Once defined the material properties as the temperature changes, the material characteristics are been set in the simulations made with PATRAN varying them according to the conditions of re-entry considered.

About loads, nodal thermal loads have been imposed on the washer, varying them according to the altitude and therefore the condition of re-entry considered. These thermal loads are listed below, they change with the altitude at which the satellite is located when re-entering in the atmosphere.

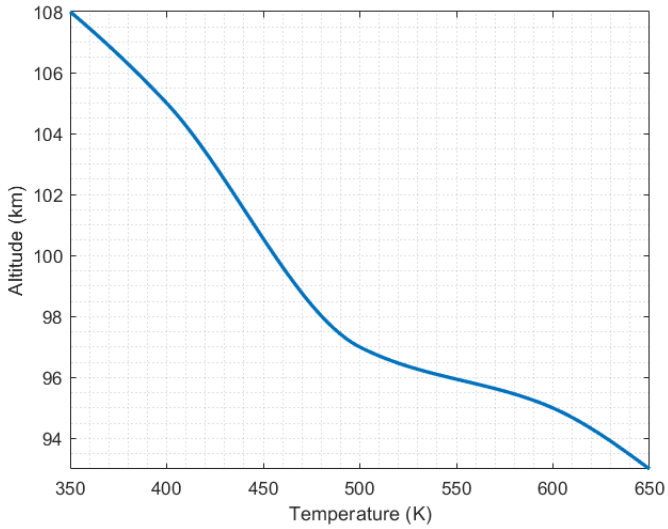

Figure 48-Washer thermal load vs altitude

In addition to the temperature, a pressure was applied simulating the preload of the screw head by about 122.321 MPa on the top of the washer and support constraints in the lower part of the washer in contact with the cleat of the demisable joint and in the inner part of the unthreaded washer where the screw is inserted.

4.2.2. Results

Setting the analyses with thermal loads and temperature-dependent material properties due to the different altitude during reentry, the underrepresented results in terms of displacements and stress were detected.

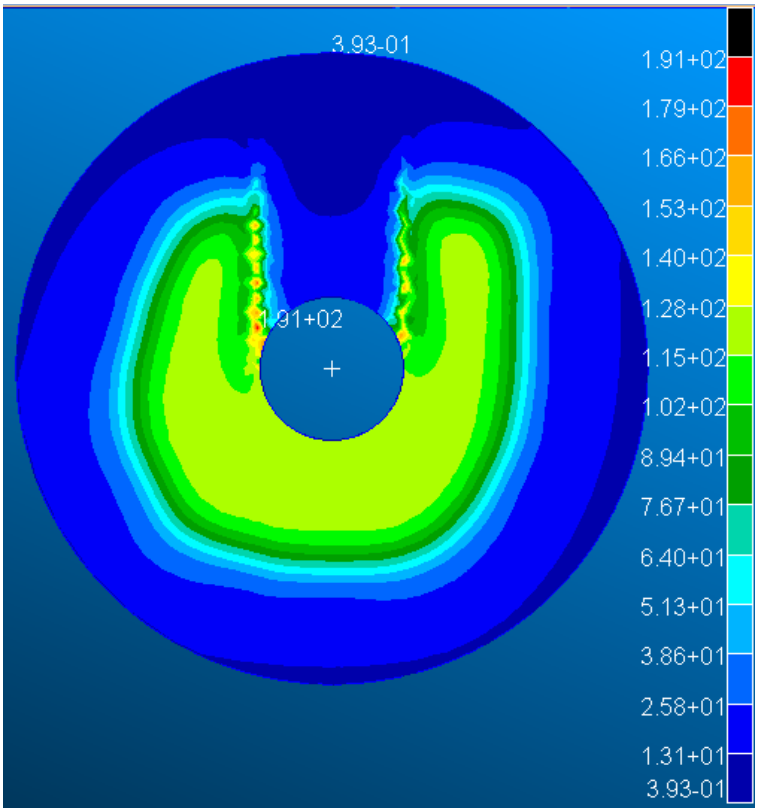

Figure 49-Washer VM Tensor map in MPa

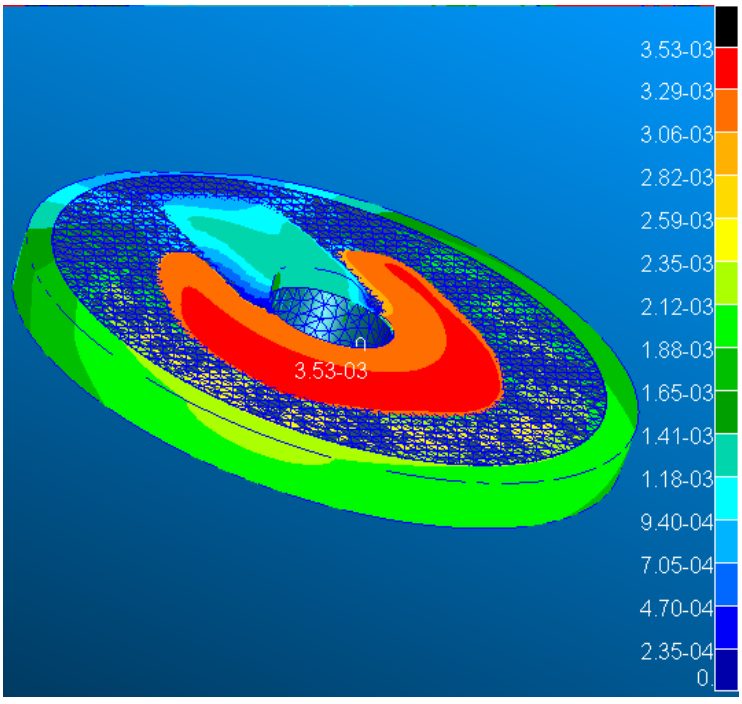

Figure 50-Washer displacement map in mm

The above results were obtained with a SOL101 at about 99 km of altitude, the washer operative conditions, with a temperature of 460K and the preload of the screw on the top of the washer that is about 122.321 MPa.
This type of solver (SOL101) performs a linear analysis in the elastic stretch of the material, so it doesn't consider the plastic zone.
The above results show that the peak of displacement and stress is in the area where the preload of the screw has been applied, with a maximum displacement of about $3 \cdot 10^{-3}$ mm and a maximum stress of about 140MPa which is less than the yield stress and therefore the washer remains in the elastic field at this altitude.
It is also clear that in the lower part of the washer, in the area near the slot of the cleat on which the washer is resting, there are points where the stress is 190 MPa and this is due to the tetragonal vertices of the mesh on which the peak stress reach a concentrated value, even if this isn't a realistic behaviour. In normal industrial practice this is an acceptable approach.
For a more accurate analysis of this study case, the complete demisable joint is been analysed with the whole assembly to verify the actual behaviour of the washer.

4.3. Demisable Joint

The third study case analysed is the demisable joint which, as illustrated in the previous chapter on washer, is a R&D part of a TASinI in Turin. This joint was used to unite the outer panels of the satellite by making sure that it remains intact at operating temperatures ca up to 130°C while breaking-up in the re-entry phase around an altitude of 90km, so that the external panels detach earlier from the satellite exposing its inner part to the thermal flow and then burning into the atmosphere without falling back to the ground and creating possible damage to people or things.
The geometry of the joint is shown below with the two cleats that accommodate the panels, the screw and the washer. Fastening the screw into the threaded cleat with the washer are fastened the two cleats and then the outer panels of the satellite.

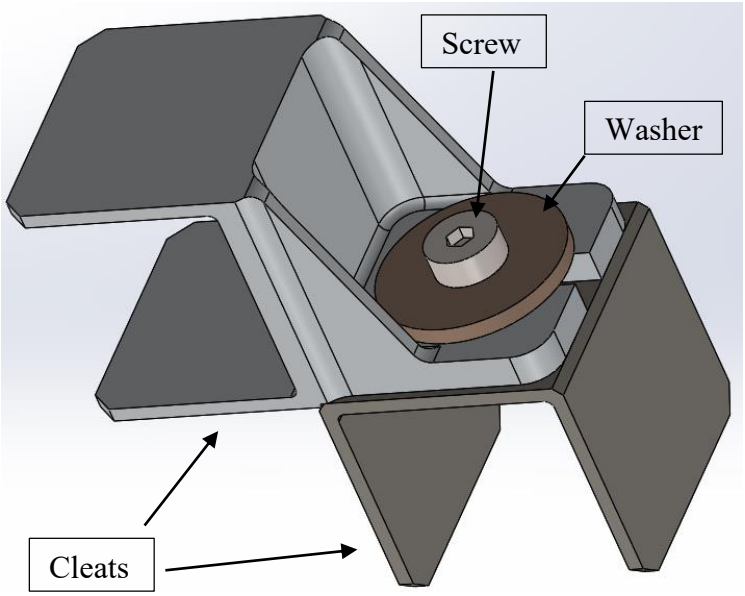

Figure 51-Joint geometry

4.3.1. Input properties

About properties of the material, the joint is made of several components: the washer in EZAC, described in the previous chapter, the screw in a titanium alloy Ti-6Al-4V and the cleat of the joint in aluminium alloy the ERGAL.
The different screw and cleat materials are described below, defining the properties of the materials according to the temperature.

Ti6Al4V

The screw is made by titanium to withstand high temperatures and mechanical stresses that the panels could sent to the joint and then lead to the breakage of the screw that holds it together.
This titanium alloy is advantageous because thanks to the main alloy elements (aluminium and vanadium) it has good stiffness to corrosion, oxidation and high mechanical resistance at high temperatures, in addition it is a very light material and therefore it is very favourable to use.

The characteristics of this alloy are illustrated below with the properties behaviour as a function of temperature.

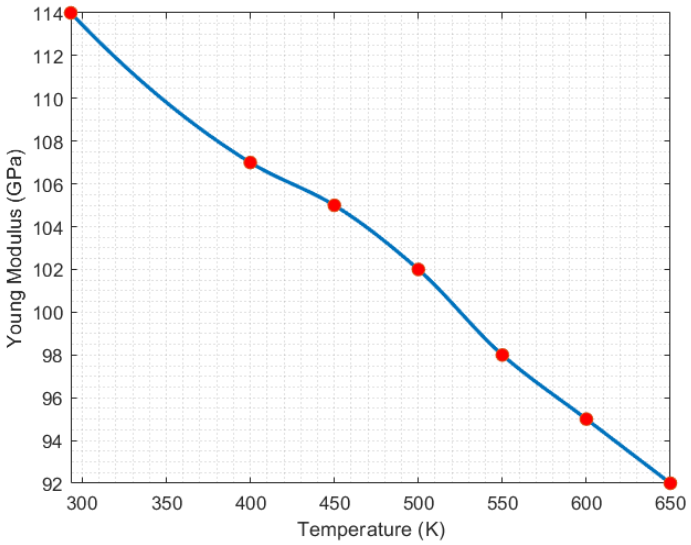

Figure 52- Elastic modulus of Ti-6Al-4V vs temperature

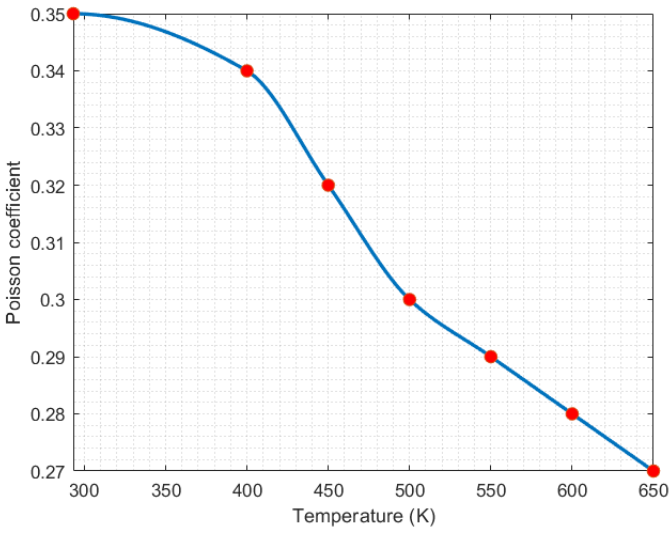

Figure 53- Poisson coefficient of Ti-6Al-4V vs temperature

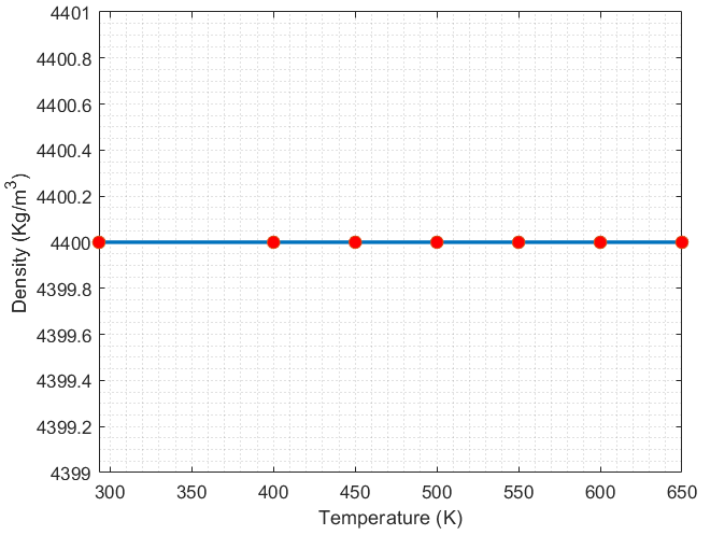

Figure 54- Density of Ti-6Al-4V vs temperature

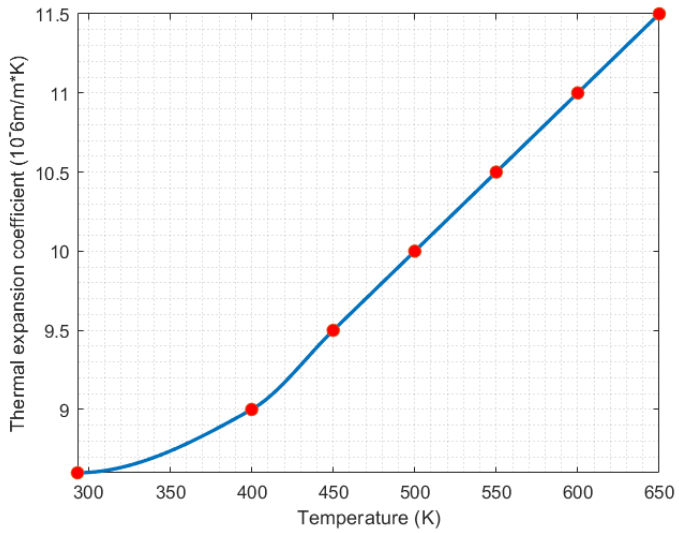

Figure 55- Thermal expansion coefficient of Ti-6Al-4V vs temperature

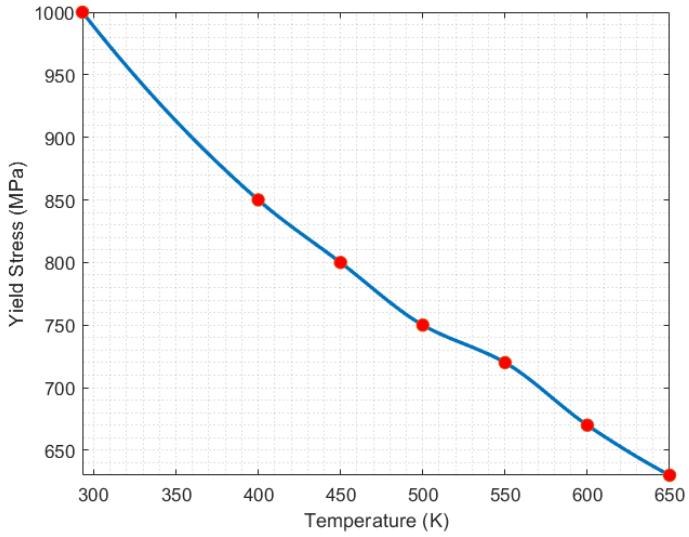

Figure 56- Yield stress of Ti-6Al-4V vs temperature

As it is logical to expect, the properties of the material decrease as the temperature increases and the material degrades as the temperature rises.

This titanium alloy, like silicon nitride, resists to high temperatures with the density that is about constant in the range considered and the coefficient of thermal expansion which results to be in the same order of magnitude of a ceramic material as the Si3N4 but with higher values because it is a metallic alloy and therefore expands more than a ceramic when subjected to thermal loads.

ERGAL

The cleats are made of Al 7075 alloy, also known as ERGAL, which is an alloy of aluminium and zinc and is the lightest of aluminium alloys, with a high resistance to shocks and stresses. This type of alloy is the least subject to thermal expansion between aluminium alloys and therefore more suitable for use in outdoor environments because it supports the sudden changes in temperature.

The trends of the characteristics of this alloy are reported according to the temperature.

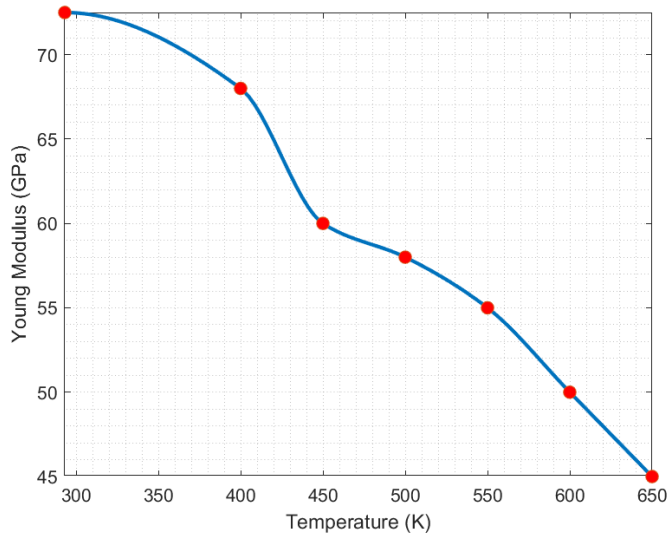

Figure 57- Elastic modulus of ERGAL vs temperature

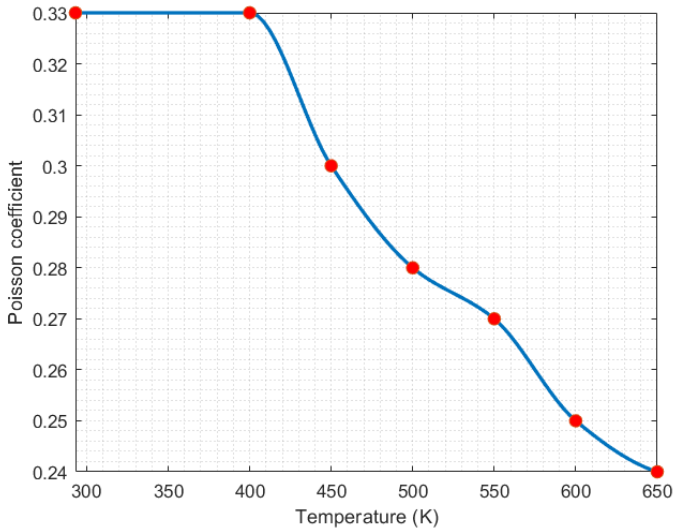

Figure 58- Poisson coefficient of ERGAL vs temperature

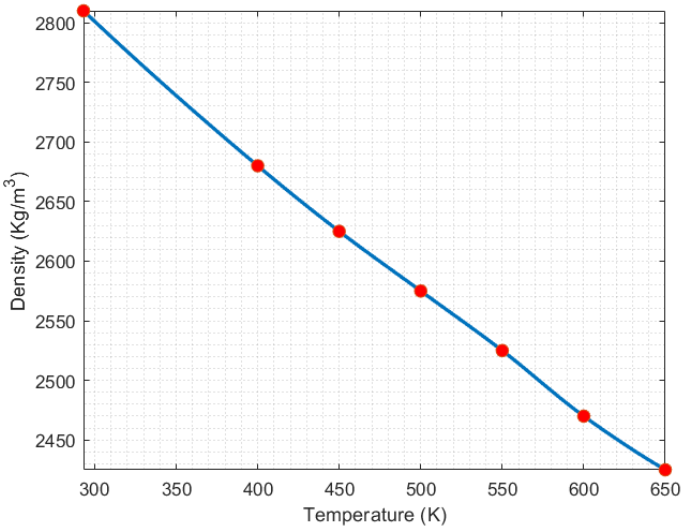

Figure 59- Density of ERGAL vs temperature

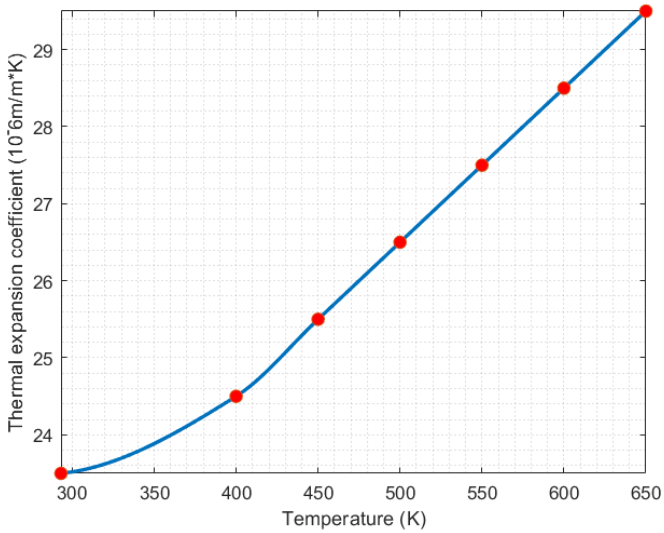

Figure 60- Thermal expansion coefficient of ERGAL vs temperature

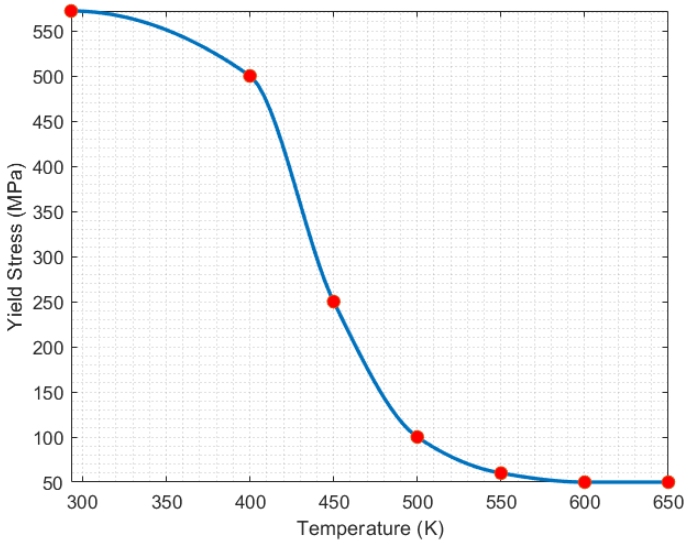

Figure 61-Yield stress of ERGAL vs temperature

From the trends of ERGAL properties it's evinced that it degrades as the temperature increases and therefore the values of its characteristics decrease.

As is also noted by the coefficient of thermal expansion, this alloy expands a lot and therefore it isn't very resistant to thermal loads such as a ceramic or a titanium alloy.

However, defined the behaviors of the different materials with the temperature, they are set on PATRAN varying according to the temperature at the re-entry.

4.3.2. Loads and contact

Regard to the loads applied on the joint it was considered a maximum temperature at operating altitude which is about 450 K applied on all the knots of the joint and the preload that the head of the titanium alloy screw exerts on the washer which is about 122.321 MPa, applied to the 3D elements in contact between the screw head and the upper part of the washer.

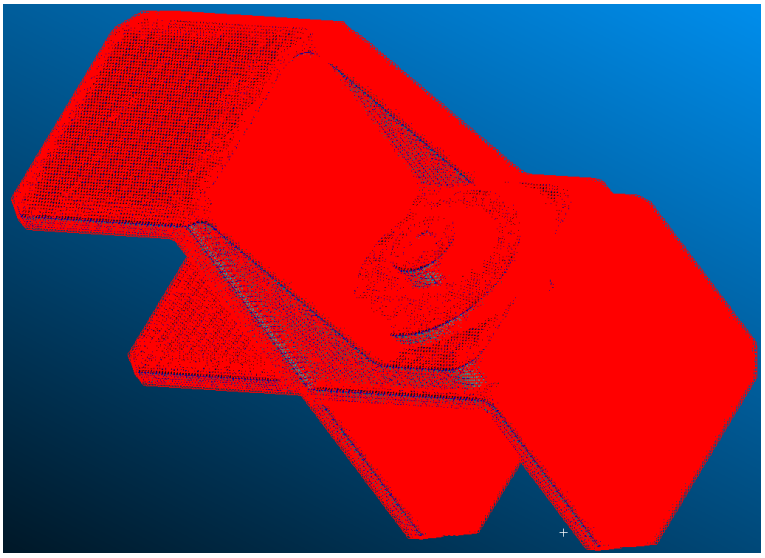

Figure 62-Temperature on knots

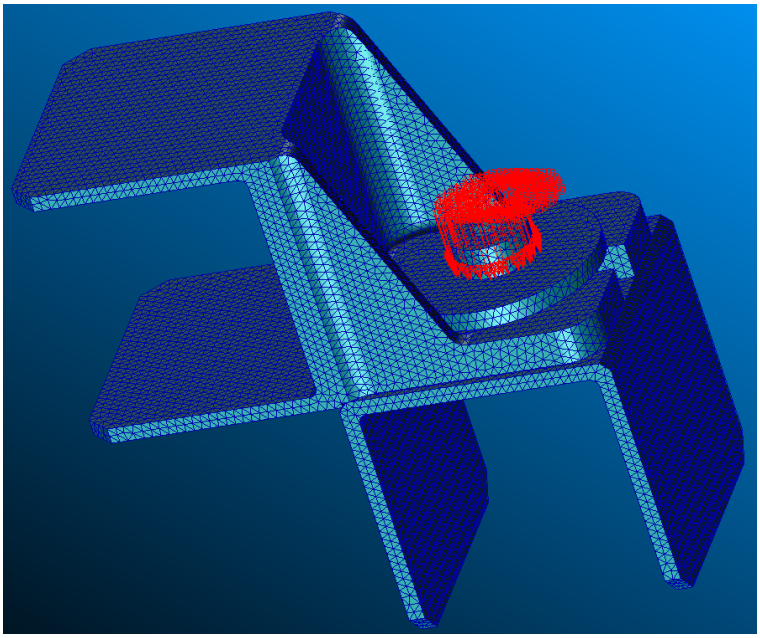

Figure 63-Preload on the washer

During orbital life, the satellite is subjected to additional forces such as linear loads or centrifugal accelerations and therefore the angular velocities and g accelerations are considered in the bottom for each altitude when re-entering in the atmosphere.

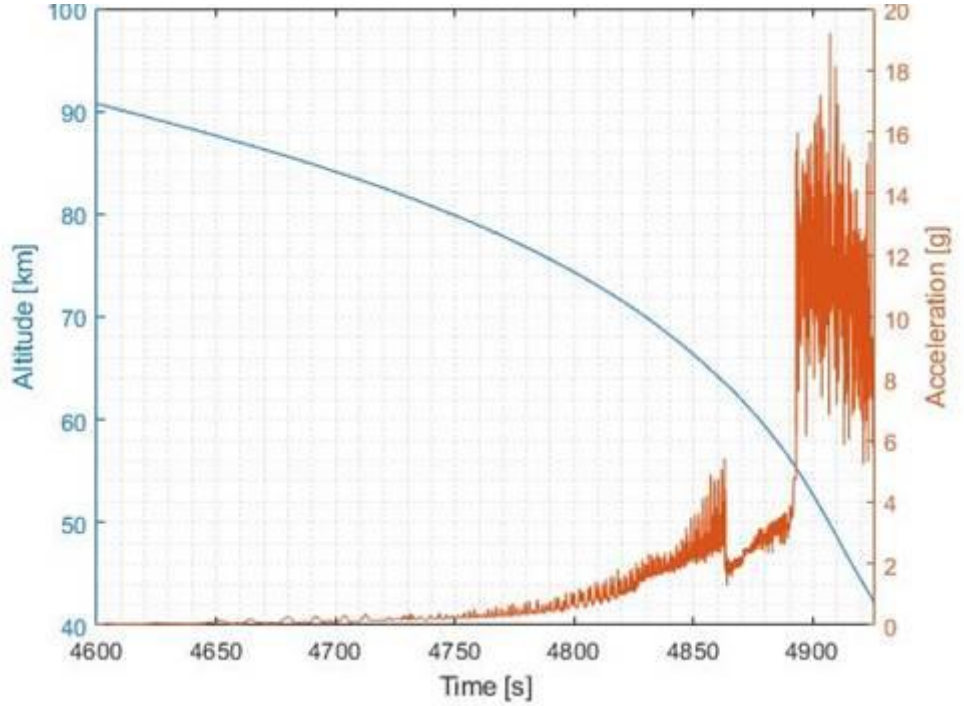

Figure 64-Linear accelerations on the Joint

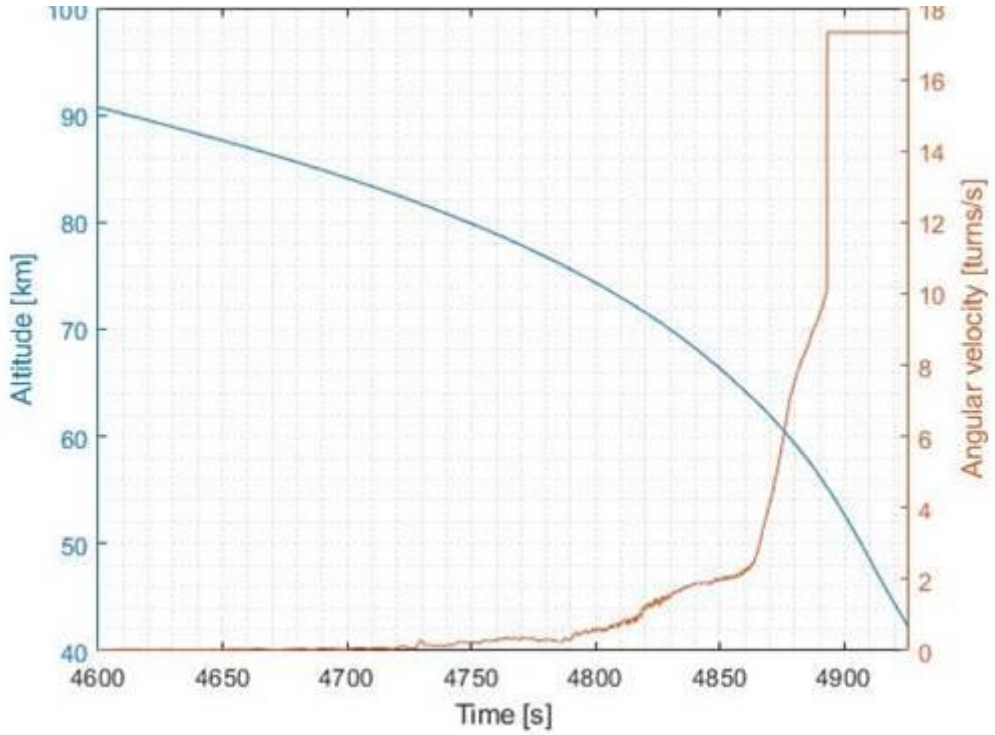

Figure 65-Angular velocities on the Joint

Can be seen that the linear accelerations and angular velocities of the satellite start to manifest substantially and then increase after the 80 km of altitude because the satellite starts a tumbling phase rolling on itself and increasing the stresses suddenly decreasing the altitude.

Regarding the constraints, wedgings are considered in the internal parts of cleats that accommodate the outer panels of the satellite thereby blocking the translations and rotations around the main axes.

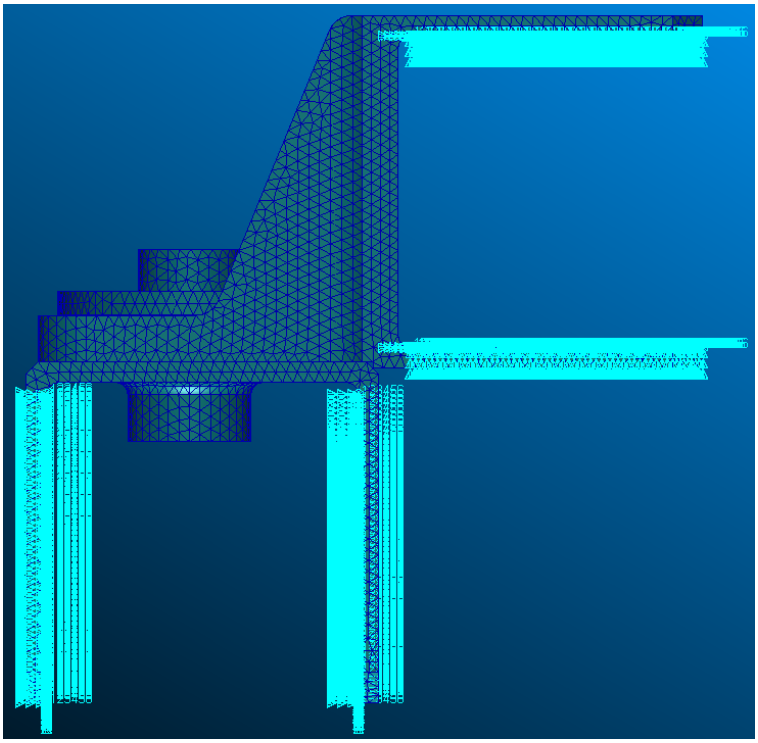

Figure 66-Constraints on the cleats

About the contacts between the various components of the joint (cleats, washer and screw), there are conditions of congruence between the nodes of the components in contact and to carry out the analysis avoiding penetrations between objects that lead to FATAL errors in the simulation, it's leaved a gap of 0.01 mm and launches the analysis verifying the results obtained with the consequent considerations.

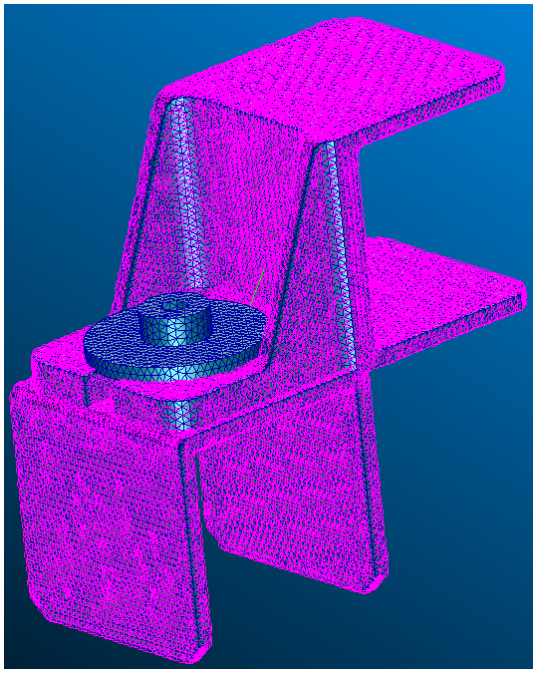

Figure 67-Contact between cleats

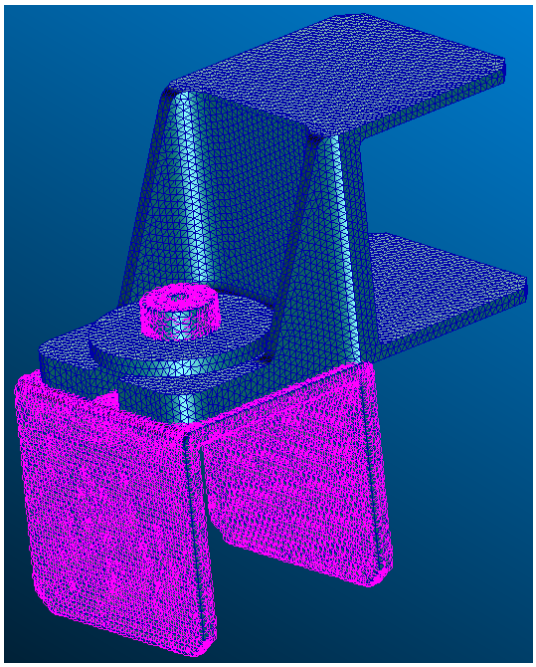

Figure 68-Contact between screw and cleat

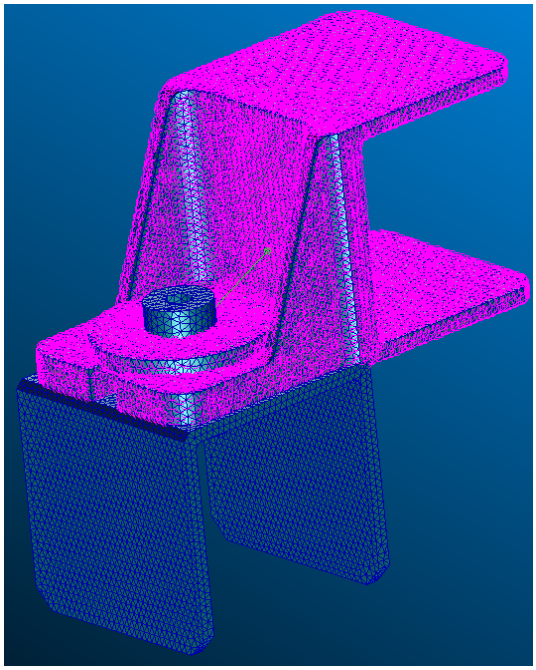

Figure 69-Contact between washer and cleat

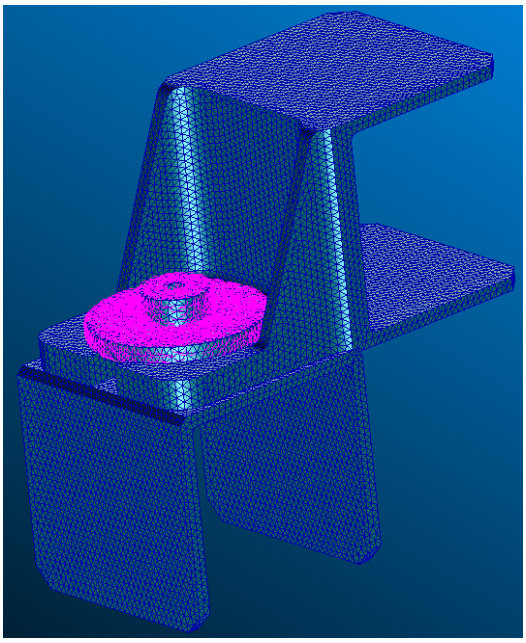

Figure 70-Contact between washer and screw

4.3.3. Results

Setting the properties of the materials, the constraints and the loads are analysed joint structural behaviour with the PATRAN software.

The analyses were performed not like the previous cases with a SOL101 solver and therefore considering only the elastic field of the material, but with SOL400 a type of solver or a nonlinear solver which also analyses the plastic field with the addition of implicit models in the analytical resolution, in which the time interval varies according to convergence.

The SOL400 solver is therefore more realistic than the SOL101 and has been chosen because the linear solver fails to guarantee a proper solution with the contacts if there are mechanical and thermal loads due to inadequate management of the thermal expansion of the material that carries the calculation to divergence.

Therefore, analysing therefore the results obtained with the SOL400, the values of the displacements and the stresses have been highlighted, in particular on the washer which is the most interesting case for the purposes of this project on the demisable joint.

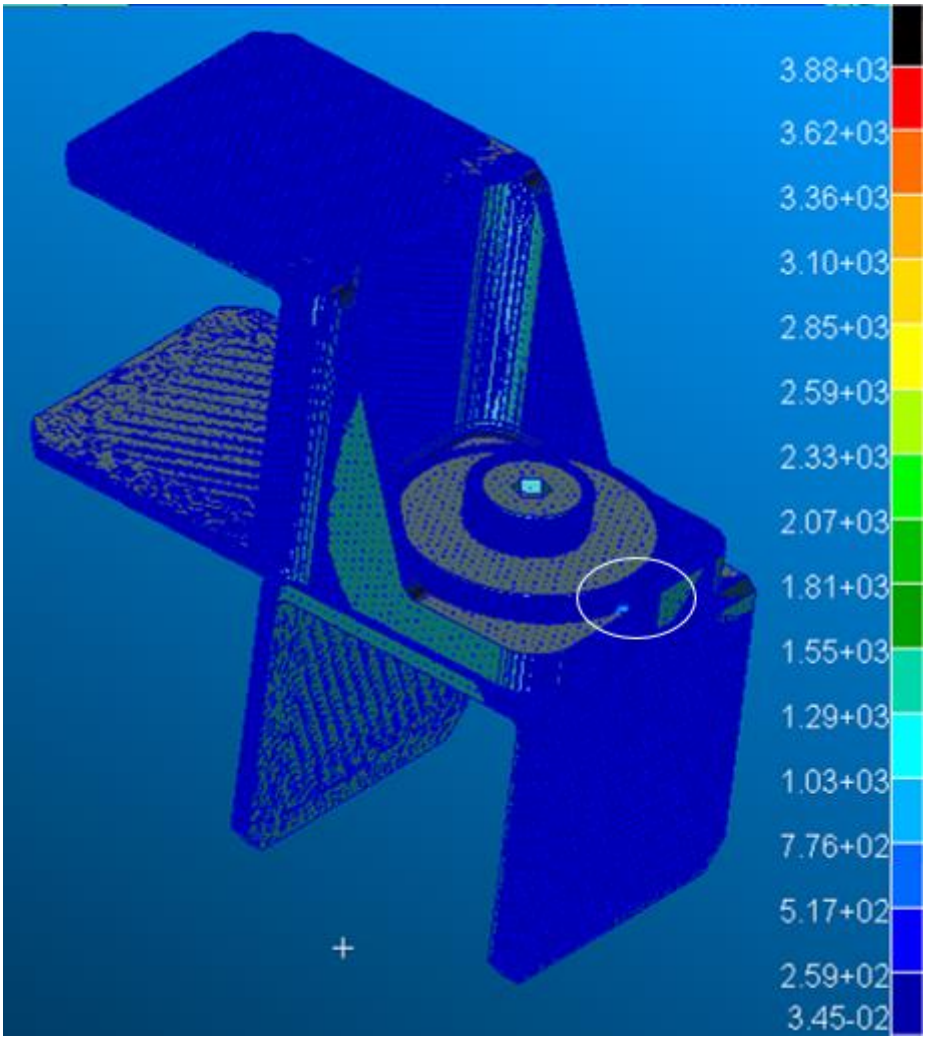

Figure 71-VM tensor stress map in MPa

The stress map on the joint shows that most of the stresses are concentrated in the area represented in blue and according to the range indicated on the side turn out to be some MPa.

In Figure 72 are highlighted Von Mises tensor, circled in the Figure 71 considering operational conditions with 450 K and about 122.321 MPa, applied to the 3D elements in contact between the screw head and the upper part of the washer.

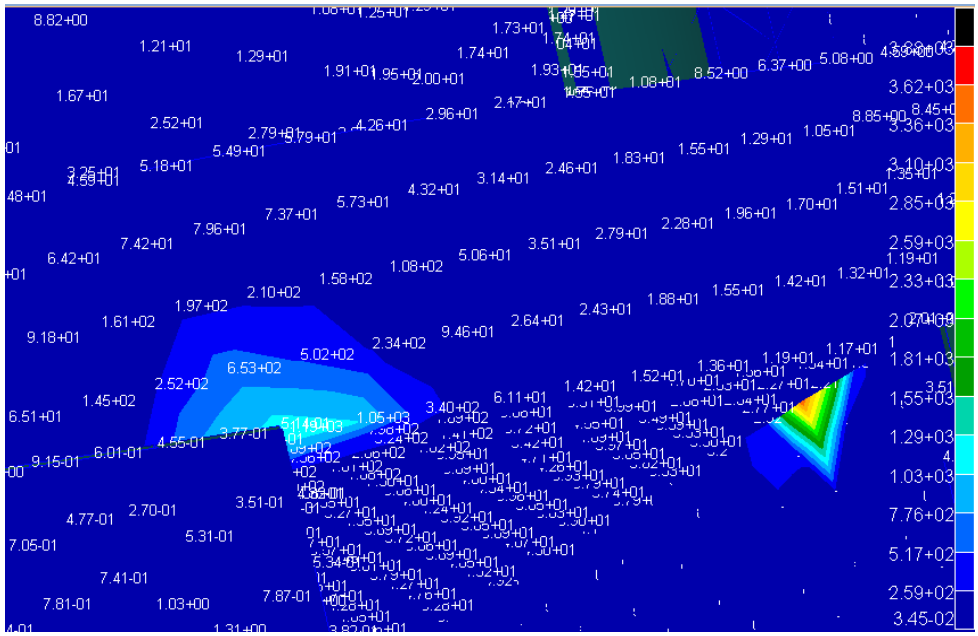

Figure 72-Washer's VM tensor stress map in MPa

Can be seen that there are peaks of stress that arrive up to some GPa and this is due to the mesh since there are uniform distribution of loads and constraints. In zones not adjacent to stress peaks it is noted that stress is higher than the limit of the elastic range of 150 MPa at 450 K, but still near to it.

Even if the actual stress exceeded the EZAC yield stress of some MPa, can be argued that the breakup of the washer is not reached. It's normal practice in industrial project to eliminate some elements that reach in concentrated zone values that aren't realistic, due to the FEM numerical approximation.

Since it has entered the plastic field, the washer shows irreversible displacements that are depicted at the bottom in millimeters.

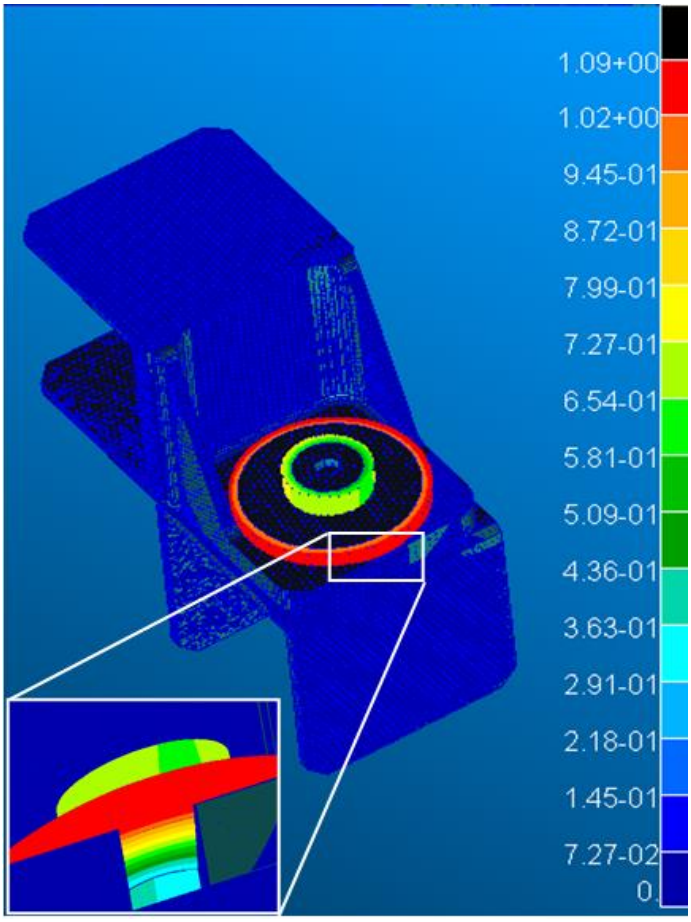

Figure 73-Displacements map in mm

Can be noted that the resulting displacements are in the order of 10^{-1} mm. By focusing on the the bottom of screw, washer and cleat can be highlighting that there are washer deformations that increasing from screw to the external radius.

4.4. Joint Test

In this chapter is described a laboratory test of a joint, like the one analysed in PATRAN and described before, in which are been used a bracket and a screw both in steel and a washer made of EZAC of the same geometry and material of that used in the Demisability Joint.

The purpose of this laboratory test was to analyse the behaviour of the washer at high temperatures when subjected to a preload of the screw on the top.
The test setup is shown in the figure below where are illustrated tools and how the washer is exposed to the thermal flow.

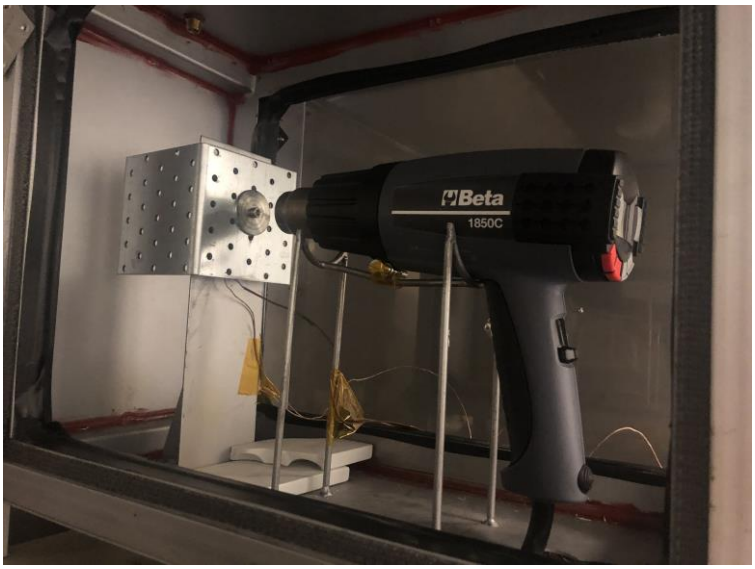

Figure 74-Test setup

For the test, a thermal gun has been placed to simulate the thermal flow when the washer re-entry in the atmosphere and centred on the screw head which is screwed into the washer with a moment of 7 Nm with screw-nut system.
It has been engraved a slot of diameter like that of the screw that pervades it (about 5mm), to simulate the cleat slot of the demisable joint.
The joint was then fastened to a bracket of a theca that was inserted in a hood to breathe the fumes from the melting of the washer.
To carry out the test, the temperature of the thermal gun has increased to its maximum limit of 650 °C and by varying the airflow up to its maximum of 500 l/min heating the washer and controlling the temperature with thermocouples placed in contact with the washer in the lower part not exposed to the thermal gun flow.
After performing the test, gradually raising the airflow and the temperature of the gun, the washer was closely observed by unscrewing it from the joint and showing that it went

into the plastic field because it has a minimum deformation in the lower part coincident with the slot of the bracket and in the upper area surrounding the screw head.

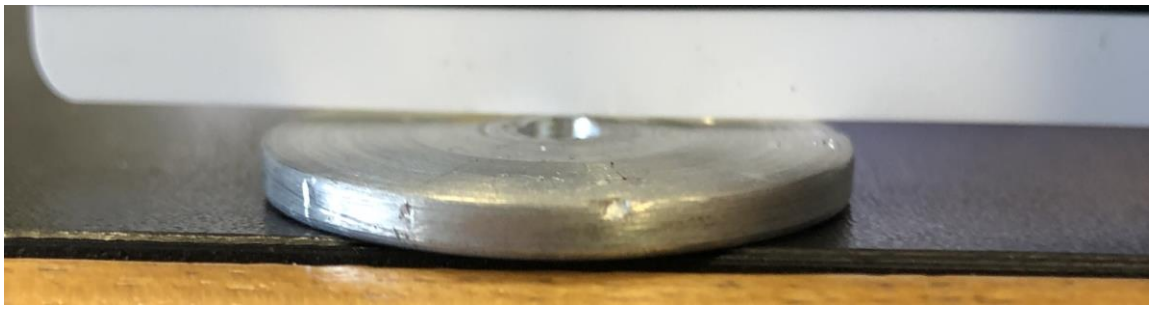

Figure 75-Washer real deformation in the lower part

Figure 76-Washer deformation in the upper part

Observing it carefully, an irreversible deformation of the washer is detected in the lower and upper part indicating that the washer has entered in the plastic field and therefore doesn't recover its original shape as in the elastic field.

It is also visible a drop that is solified after melting of the material, at about 650 °C, in the lower part of the top face of the washer.

This test goes ahead to the validation of the simulations carried out in PATRAN even if with a joint geometry and different loads between the bracket and the washer, but nevertheless can be detected a plastic deformation in the zones near the slot and the head of the screw.

5. FEM simplification

In this chapter are described alternative methods to FEM to analyze from the structural point of view some components of the satellite. Due to the complexity at the computational level, FEM takes a lot of time to analyze a whole satellite to the destructive re-entry to the atmosphere and to perform a FEM analysis for each moment at the re-entry is very expensive in terms of time. Therefore, for the structural analysis of a satellite are hereinafter summarized potential alternative methods for reducing calculation time even if there are strong approximations in modelling some components with simple models such as beams or plates.

One potential way is start focusing on the components which drive the atmospheric re-entry: e.g. some external components such as solar arrays or CSAR radar of the Sentinel-1 satellite are bulky from the point of view of re-entering to the atmosphere because they change, when detaching, the ballistic behaviour of the satellite and it is important to have an idea of the altitude at which they are detached; as well as the external panels that, when detaching, expose the internal components of the satellite to the external flux.

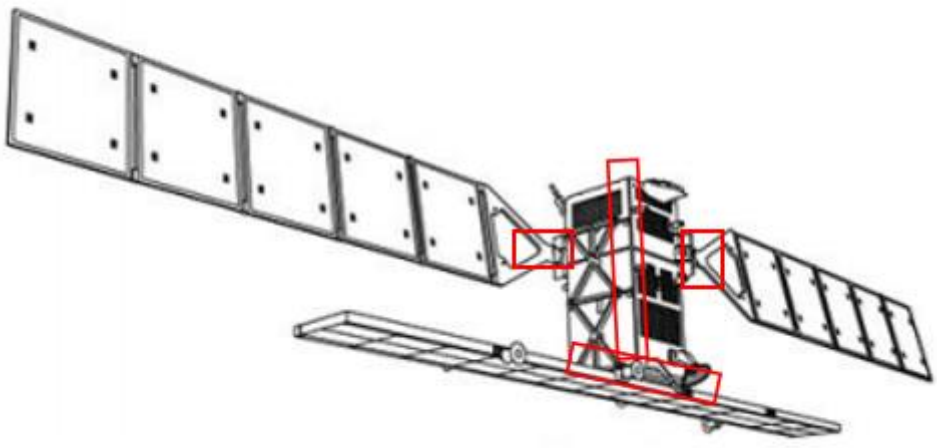

Figure 77-Sentinel-1 representation

In the Sentinel-1 representation have been highlighted the brackets of solar panels and CSAR that can be approximated as beams and external panels, considered as plates.
For example, for an external satellite panel with a mesh given in a FEM tool and with different temperatures for each element, it will be approximated as a plate with an average temperature and the constraints it has in the satellite.
From the structural point of view of the destructive re-entry, the internal components are not subjected to high stress as e.g. the external appendixes, but they disintegrate in the atmosphere except for components such as bench or tanks or other elements that resist at high temperatures.
Even if the number of interesting items is limited, an unusual FEM analysis would be unsuitable for atmospheric re-entry simulation, since it would require to be repeated at each time step of simulation, which would lead to simulations lasting for at least several weeks.
Another possible simplification to the analyses is to reduce the calculation time by using 2D elements instead of the 3D ones, having fewer knots and halve almost the time of the simulations, but the time of FEM simulations would be still high.
A further way is to run the FEM analysis in critical conditions of the re-entering, analyzing the components with a 2D mesh to have an idea of the breaking behaviour of the analyzed component. This technique would be limited only to re-entry-driving components.
Some codes, like the previously mentioned SCARAB [4], to get the stress in the various elements of the satellite, apply secant planes exclusively for few simple elements like the arm that link the satellite to a solar panel and therefore, being approximated to a beam; it can be analyzed with the Navier expression:

- Normal stress:

$$\sigma = \frac{F_x}{A} + \frac{M_y z}{J_y} + \frac{M_z y}{J_z}$$

- Tangential stress:

$$\tau = \frac{M_x \rho}{J_P}$$

Where:

F_x is the stress in x direction (axial direction);

A is the cross section;

M_y the bending momentum;

M_z the torque moment;

J_y the momentum of inertia around the y-axis;

J_z the momentum of inertia around the z-axis;

J_P the polar momentum of inertia;

ρ radius of inertia;

To understand if the analyzed component has come to breakup, the equivalent stress of Von Mises is compared with the UTS of the material and if VM stress exceeds the UTS, the component is considered broken.

Therefore, an option could be start from what was done on SCARAB and extend the model to other components that are decisive for the fragmentation of the satellite.

As far as temperatures are concerned, the SCARAB software doesn't do any analysis except to eliminate mesh elements that exceed the melting temperature of the material.

However, a simplified expression can be used in which the stress of each mesh element is proportional to the elastic coefficient matrix [Q], the temperature jump ΔT, the vector of mechanical deformation $\{\epsilon_m\}$ and the thermal expansion coefficient α, for the various elements:

$$\{\sigma\} = [Q]\{\epsilon_m\} - [Q]\{\alpha\}\Delta T$$

It's important to consider a congruence relationship between the various mesh elements because they are interconnected and the temperature jump should be considered from the

minimum, usually at ambient temperature, to the maximum one to which it arrives during re-entry.

The stress on each mesh element is substantially given by mechanical loads (aerodynamics, inertia forces and distributed stresses) and by thermal loads that affect each section of the satellite, varying during the re-entry and leading to thermoelastic loads.

Therefore, for simple shapes such as a beam or a plate, it is possible to apply Navier or the above-mentioned plate model, otherwise the FEM can be used with comparison values visible from those obtained in the simulations previously described in the chapter of the study cases.

6. Conclusions and future developments

The theme of the atmospheric re-entry is a topic studied in recent years and TASinI in Turin develop a dedicated low fidelity code of re-entry and started activities aimed at achieving spacecraft-oriented tool.

The analyses carried out in this thesis project and described in the study cases chapter are a starting point for the understanding of the tensional state on a satellite in orbit and its structural behaviour when re-entering the atmosphere. Three different study cases have been analyzed to the destructive re-entry to the atmosphere (a bench, a washer and a joint) and it is evident that they get influenced by re-entry concerning structural behavior.

The bench, which is a component made of ceramic material, is difficult to disintegrate due to its high resistance to elevated temperatures and because it is placed inside the satellite well shielded by different components as e.g. the external panels.

The washer and consequently the joint behave differently than the bench since they are made of metal alloys and are placed externally to the satellite, receiving a direct aero-thermic flow, and therefore easy demisability to re-entry in atmosphere with characteristics of deformation and stress different from a component made on ceramic material.

From the analyses carried out with the PATRAN software for FEM analysis it is clear that the bench fragments between the 80 km and the 90 km while the joint, and therefore the washer, does not enter in the plastic field, breaking-up at operational altitudes around 100 km.

To have an idea of comparison and for a validation of the results obtained with PATRAN, a laboratory test was carried out on the joint, focusing on the behaviour of the washer. At 650 °C the washer had entered in the plastic field starting to melt and there are displacements like those highlighted in PATRAN with a deformation in the part near the slot and close to the head of the screw.

From the analyses carried out on the study cases can be obtained an idea on the structural behavior to the atmospheric re-entry of the components, since the structural behaviour of the S/C is currently studied only at launch and in orbit lifetime, also this analysis is a

reference for the simplifications of existing structural models, as described in the FEM simplification chapter, highlighting the use of Navier or plate model for relevant elements (w.r.t. the results of the re-entry) such as reticular reinforcement structure, solar panel attacks with satellite or for the outer panels of the satellite.

About the future study fields of this project it is possible to analyses other types of components such as sandwich panels or joints inside the satellite and then shielded upon re-entry.

Another possible development of this work is the realization of an algorithm to implement on TADAP and able to carry out with simplifying methods, like those described in the chapter FEM simplification, a preliminary analysis of the structural behaviour of a satellite with calculation times lower than that of FEM.

7. Bibliography

[1] Erasmo Carrera: “Fondamenti sul calcolo di strutture a guscio rinforzato per veicoli aerospaziali”, Levrotto e Bella, Torino.

[2] J. Annaloro, P. Omaly, V. Rivola, M. Spel: “Elaboration of a new spacecraft-oriented tool: PAMPERO”, CNES, Toulouse.

[3] Gallis P.: “Atmospheric Re-entry Vehicle Mechanics”, Springer Berlin Hidelberg, New York.

[4] G. Koppenwallner, B. Fritsche, T. Lips, H. Klinkrad: “SCARAB-A multidisciplinary code for destruction analysis of spacecraft during reentry”, HTG, Katlenburg-Lindau.

[5] B. Fitsche, H. Klinkrad, A. Kashkovsky, E. Grinberg: “Spacecraft Disintegration During Uncontrolled Atmospheric Entry”, Elsevir Science Ltd, London.

[6] B. Fritsche: “Spacecraft disintegration during uncontrolled atmospheric Re-entry”, ESOC, Lindau.

[7] Pierre Omaly, Martin Spel: “DEBRISK, a Tool for Re-entry Risk Analysis”.

[8] R.W. Detra, N.H. Kemp, and F.R. Riddell: “Addendum to Heat Transfer to Satellite Vehicles Reentering the Atmosphere-Jet Propulsion”.

[9] H. Klinkrad: “ESA Space Debris Mitigation Handbook”, European Space Agency.

[10] T. Lips, B. Fritsche: “A comparison of commonly used re-entry analysis tools”.

[11] Allen, H. Julian, Eggers: “A Study of the Motion and Aerodynamic Heating of Ballistic Missiles Entering the Earth's Atmosphere at High Supersonic Speeds”, NACA Annual Report (NASA Technical Reports).

[12] Thomas P. Sarafin, Willey J. Larson: “Spacecraft structures and mechanism-From concept to launch”, Managing Editor.

[13] Johannes Gelhaus: “Upgrade of ESA’s Space Debris Mitigation Analysis Tool Suite”, Final report ESA.

8. Acknowledgements

I thank my company supervisor Roberto Destefanis and Simone Bianchi and their colleagues Marina Bellini and Stefano Destefanis for following me throughout the thesis work.

I am grateful to my academy supervisor Paolo Maggiore and Salvatore Brischetto for giving me the opportunity to do this thesis work to the fullest.

A special thanks to my parents for giving me the opportunity to reach this goal and always supporting me by being close to me even though physically distant.

A special thought to my super-sister Gabriella for guiding me during these years and for being my reference model to inspire me.

With affection I would like to thank my girlfriend Chiara for having supported me morally to the end, having shared moments of anxiety and happiness with me and always being by my side, supporting me with love and dedication, encouraging me to give my best especially in the most critical situations.

A special thanks to my "brother" Michele for having always been close to me and supporting me by encouraging me to give my best and never give up.

Furthermore, I am grateful to the Borghi and Giammarino families for making me feel part of them and having me hosted as their member.

A special thought to all my colleagues of the Polytechnic, with whom I had the pleasure of sharing joys and sufferings during all these years, in particular the friends of Nice, the group "P.I.C.", Carmine Dario Vastola, Marco Campagnoli and Mauro Mancini.